

NASA Technical Paper 1023

The ATS-6 Power System:
Hardware Implementation
and Orbital Performance

CASE FILE
COPY

Thomas A. LaVigna and Franklin L. Hornbuckle

SEPTEMBER 1977

NASA

NASA Technical Paper 1023

The ATS-6 Power System: Hardware Implementation and Orbital Performance

Thomas A. LaVigna
Goddard Space Flight Center
Greenbelt, Maryland

and

Franklin L. Hornbuckle
Fairchild Space & Electronics Company
Germantown, Maryland



National Aeronautics
and Space Administration

**Scientific and Technical
Information Office**

1977

This document makes use of international metric units according to the Systeme International d'Unites (SI). In certain cases, utility requires the retention of other systems of units in addition to the SI units. The conventional units stated in parentheses following the computed SI equivalents are the basis of the measurements and calculations reported.

The material in this document was presented in abbreviated form, at the Eleventh Intersociety Energy Conversion Engineering Conference, September 12 to 17, 1976, Stateline, Nevada.

FOREWORD

The very successful operation in orbit of the Applications Technology Satellite 6 (ATS-6), the last in the ATS series, is a tribute to its designers.

The highly adaptable ATS-6 power system interfaces with over 20 technical and scientific experiments, and allows multiple operation of these experiments and operation of the subsystems of the spacecraft without induced or coupled electromagnetic interference. Loads handled vary from peak power demands of up to 800 watts, some 200 watts in excess of the solar array capability, to the minimum base load of 150 watts.

The unique shunt-boost configuration provides direct transfer of power from the solar array to the varying loads and to shunt power dissipators for thermal control and for system regulation.

The experiments conducted with this versatile spacecraft have contributed a great deal of information that is now being evaluated for application in many technical and scientific fields. Only the future will tell us just how vast is this new knowledge. Third year experiments have already begun and we can look forward to more exciting developments from this "star" of the ATS series.

J. P. Corrigan
Deputy Project Manager/Technical
Orbiting Satellites Project
NASA Goddard Space Flight Center

CONTENTS

	<i>Page</i>
ABSTRACT	i
FOREWORD	iii
INTRODUCTION	1
POWER SYSTEM DESCRIPTION	2
HARDWARE IMPLEMENTATION	5
Solar Array	5
Electronics	12
Batteries	16
PERFORMANCE CHARACTERISTICS	18
Dynamic Regulation	19
Output Impedance	22
Overload Protection	23
ORBITAL PERFORMANCE	27
Solar Array	27
Electronics	29
Battery Performance	31
CONCLUSIONS	37

ILLUSTRATIONS

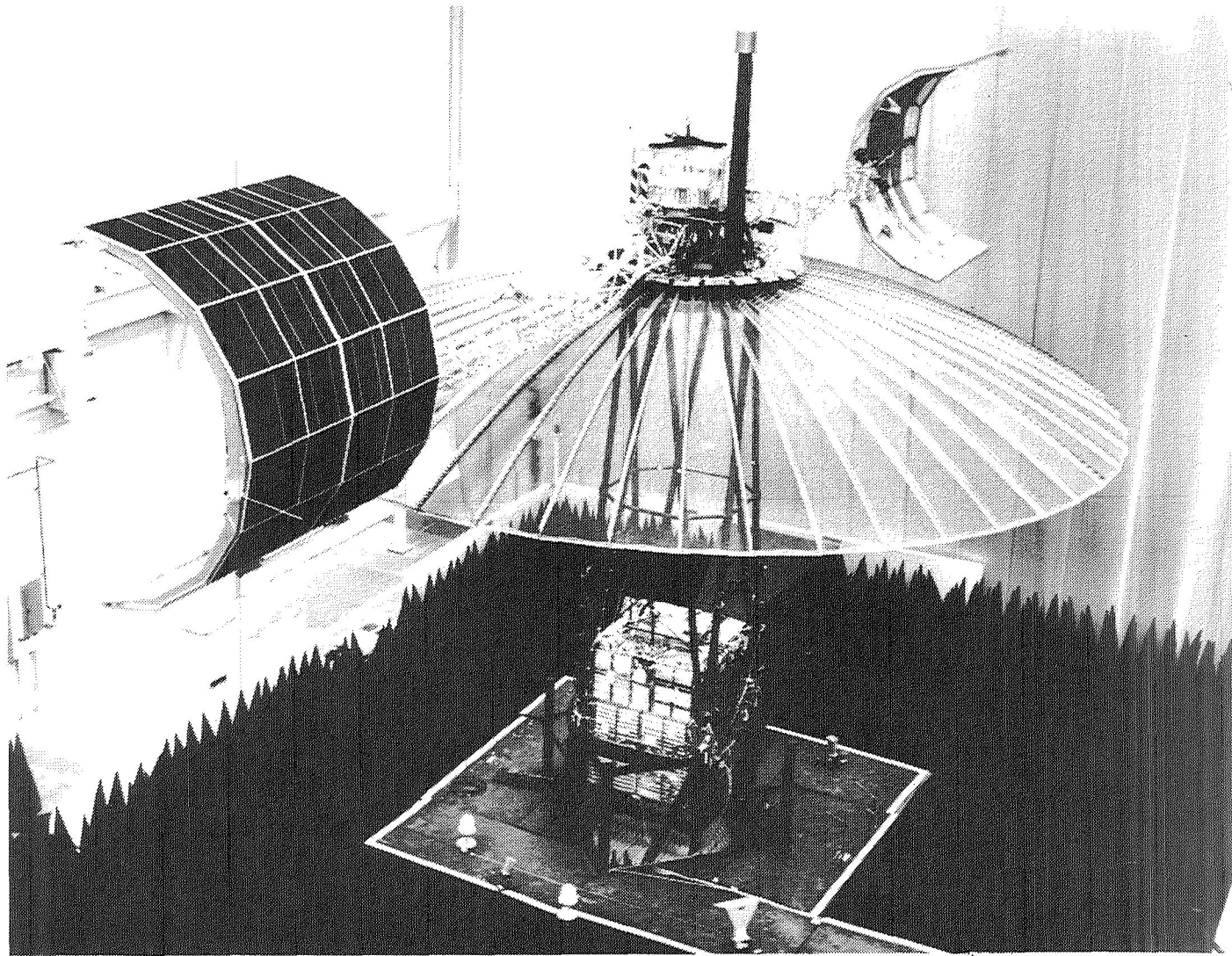
<i>Figure</i>		<i>Page</i>
1	ATS-6 configuration in orbit	1
2	Block diagram of the power system components	2
3	Functional block diagram of the power subsystem	3
4	Basic block diagram of the shunt-boost system	3
5	Regulation control modes	4
6	Solar array semicylinder	5
7	Solar array semicylinder showing a cell string	6
8	Solar panel temperature profile	7
9	Solar cell stack	8
10	Panel electrical performance versus thermal vacuum cycles	9
11	Test setup for solar array flash illumination	10
12	String I-V curve	11
13	The power regulation unit	13
14	150-watt load interface circuit	14
15	The power control unit	14
16	A shunt dissipator	15
17	Solar array schematic diagram	17
18	The battery assembly	18

ILLUSTRATIONS (continued)

<i>Figure</i>		<i>Page</i>
19	Dynamic regulation (shunt mode) 500-watt solar array	20
20	Dynamic regulation (shunt/boost mode) with 400-watt solar array	20
21	Dynamic regulation (boost mode) with 0-watt solar array	21
22	Output impedance	22
23	PCU timing scheme for bus protection	23
24	Bus response to nonessential bus overload	24
25	Bus response to essential bus overload	25
26	Regulation characteristics of the LIC	26
27	LIC input ripple voltage attenuation vs frequency	26
28	Load interface circuit output impedance	27
29	Measured solar array power	28
30	Regulated bus data	30
31	Preflight deadbands	31
32	Battery discharge profile for SITE operations	34
33	Battery discharge curves for eclipse seasons #1 through #6	34
34	Battery charge characteristics	36
35	Discharge characteristics	36

TABLES

<i>Table</i>		<i>Page</i>
1	Electrical and Mechanical Panel Characteristics	6
2	Materials Used in the Solar Cell Stack	8
3	Sizes, Weights, and Power Handling Capability of Electronics Components	12
4	Dynamic Regulation Requirements	19
5	Electrical Power System: In-Orbit Performance	30
6	Shunt Dissipator Power Sharing	32
7	Battery Discharge Cycles	33



Frontispiece. The flight model of the Applications Technology Satellite 6.

THE ATS-6 POWER SYSTEM: HARDWARE IMPLEMENTATION AND ORBITAL PERFORMANCE

Thomas A. LaVigna
NASA Goddard Space Flight Center

Franklin L. Hornbuckle
Fairchild Space & Electronics Co.

INTRODUCTION

Since May 1974, the Applications Technology Satellite (ATS)-6 has been conducting unique communications experiments from its geosynchronous equatorial orbit.

ATS-6 carries a 9.1-m (30-ft) parabolic antenna (figure 1) that allows signals to be transmitted to Earth at an effective isotropic radiated power (EIRP) in excess of 200,000 watts (50 dBW). This dramatic increase in EIRP over previous satellites allows direct transmission of high quality signals on multiple frequencies to small and inexpensive ground receivers. To date, ATS-6 has successfully conducted more than 20 meteorological, technological, communications, and scientific experiments.

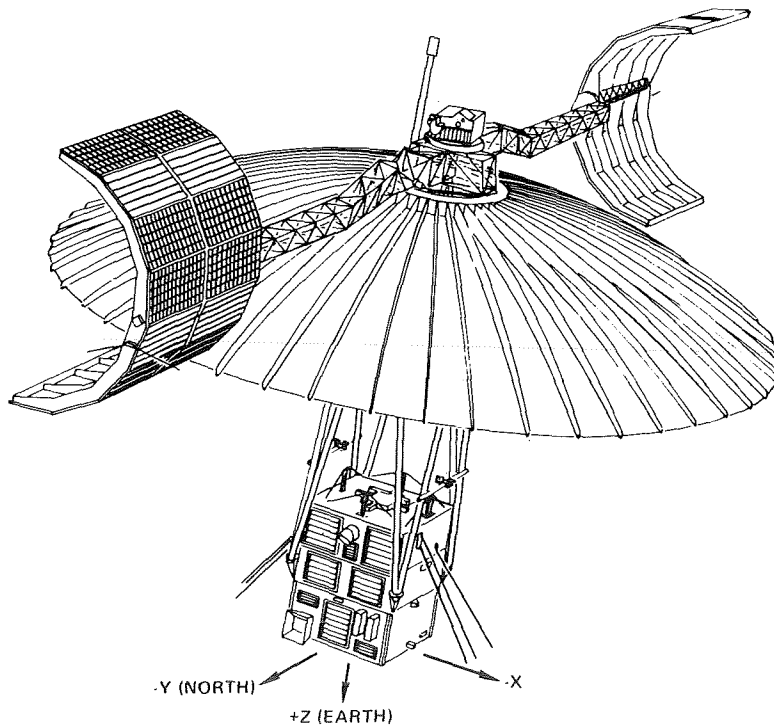


Figure 1. ATS-6 configuration in orbit.

The satellite, built by Fairchild Space and Electronics Company under the direction of NASA Goddard Space Flight Center, has demonstrated the relay of health and educational TV programs to isolated communities, conducted maritime and aeronautical traffic control and position location experiments, tracked and relayed data to and from low orbiting satellites (Apollo-Soyuz, GEOS-3 and Nimbus 6), gathered meteorological data, investigated RF interference, measured charged particles and spacecraft charge potential in orbital environment, and performed other experiments. The excellent performance of the power system has contributed significantly to this successful mission. Its flexibility has allowed multiple operation of experiments including load power demands greater than the power available from the solar array. The power system can efficiently provide up to 1000 watts. At present it has supplied peak power demands of up to 800 watts, some 200 watts in excess of the capability of the solar array.

POWER SYSTEM DESCRIPTION

The power system consists of two cylindrical solar array paddles, two nickel-cadmium batteries, a power control unit, a power regulation unit, twelve shunt dissipators, a squib interface unit, seven load interface circuits, and a 10-m (35-ft) array harness.

The system components are shown in figure 2, and a detailed functional block diagram is shown in figure 3. Figure 4 shows a simplified block diagram of the shunt-boost configuration used by the power system. The shunt-boost system provides maximum use of solar

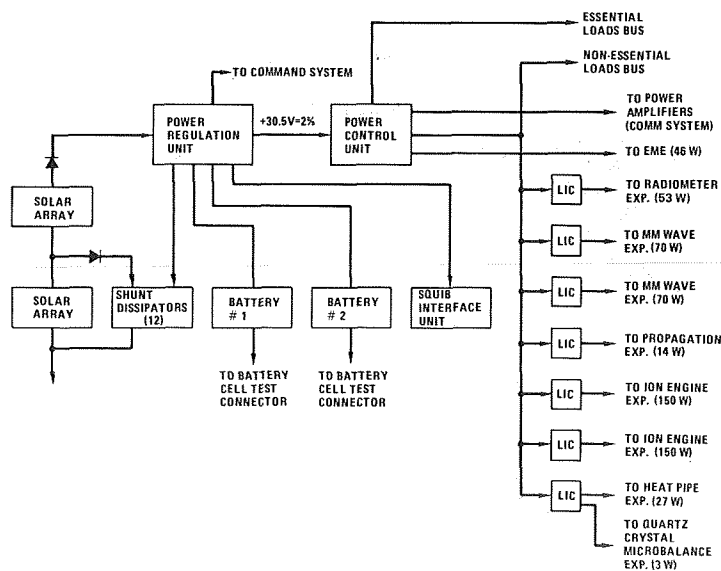


Figure 2. Block diagram of the power system components.

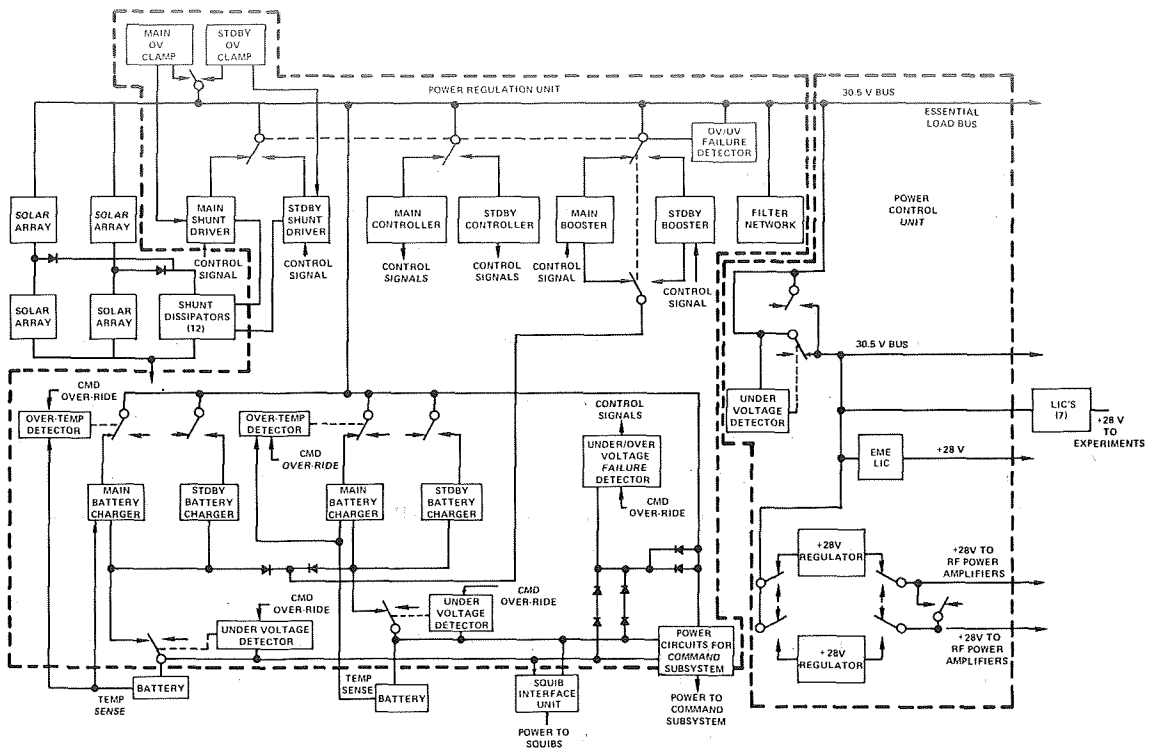


Figure 3. Functional block diagram of the power subsystem.

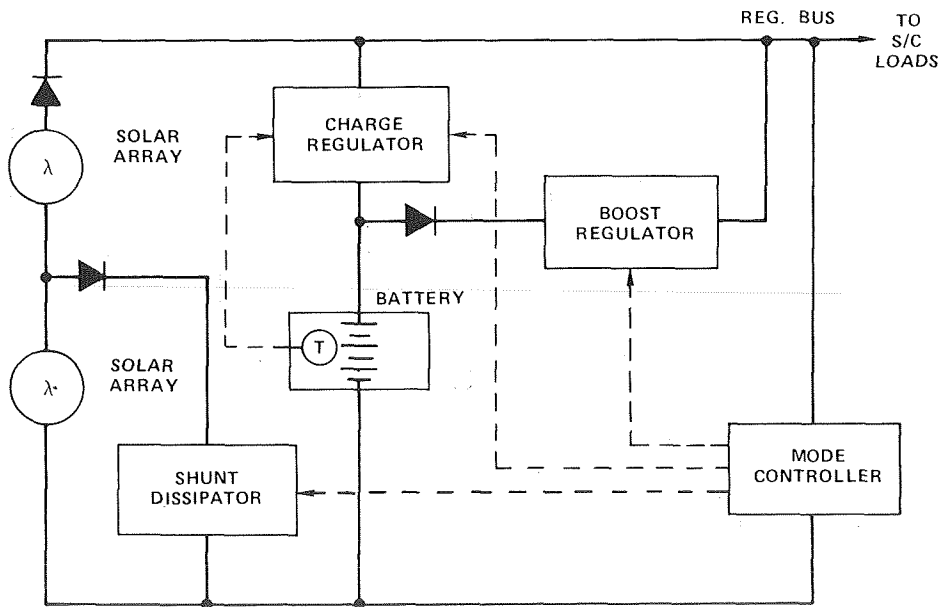


Figure 4. Basic block diagram of the shunt-boost system.

array power by operating the array at a fixed voltage where essentially maximum power is available. If the power demanded by the load exceeds the power that can be supplied by the array, the array continues to deliver maximum power with the batteries providing the deficiency.

Primary power to the system (up to 600 watts) is provided by the solar array directly to the spacecraft power bus. Excess power from the solar array is stored in the two batteries or dissipated in the shunts when the battery charge requirements are exceeded.

The main bus is regulated to a level of 30.5 Vdc \pm 2 percent. The solar array voltage is regulated by partial shunt regulation, and the battery voltage is regulated by a boost regulator.

The battery chargers are enabled to charge the batteries when excess power is available from the solar array. Each battery has separate charge control circuits and is normally charged using a current limited (1.5 amp maximum, C/10) rate with temperature compensated voltage control. When the power from the array exceeds both the load power and the charge requirements of the batteries, the excess is dissipated by the shunts.

A common controller provides the necessary error signals for the three major modes of operation; they are the shunt, charge, and boost modes. These functional modes, shown in figure 5, provide the regulation and the charge control for the power system.

Secondary power conditioning at 28 Vdc is provided for the solid state RF power amplifiers and for each experiment through individual load interface circuits. Load interface circuits provide on-off control, overload protection, noise suppression, and line isolation.

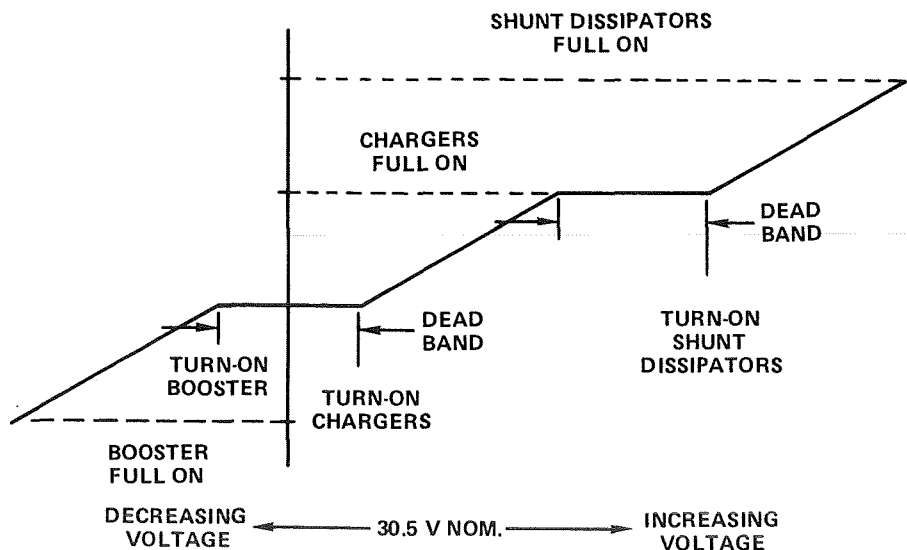


Figure 5. Regulation control modes.

HARDWARE IMPLEMENTATION

Solar Array

The solar array (see figure 1) consists of 21,600 solar cells distributed on two semicylindrical assemblies [each weighing 32.89 kg (72.5 lb)] mounted on booms parallel to the north and south axes of the spacecraft. There are 32 panels in the entire array, arranged in a double row, resulting in a 16-sided prism. The normal to each of these facets is at an angle of 22.5 degrees with respect to the normal of the adjacent face. With this large number of facets, the power output of the solar array is nearly constant throughout the orbit, geometric factors introducing only a ± 0.15 percent variation. A photograph of an array semicylinder is shown in figure 6.

The solar cells are arranged in 96 strings of 3 parallel by 75 series cells each, with isolation diodes connecting each string to the power bus. There are 3 series strings on each panel (a total of 675 solar cells per panel) plus 2 parallel isolation diodes per string (figure 7). The cells are arranged three rows to each string, and the direction of current flow is alternated to reduce the external magnetic field. The taps for the shunt dissipators are made at a point 50 cells from the negative bus, which corresponds to the end of a row of solar cells. Table 1 gives the electrical and mechanical panel characteristics.

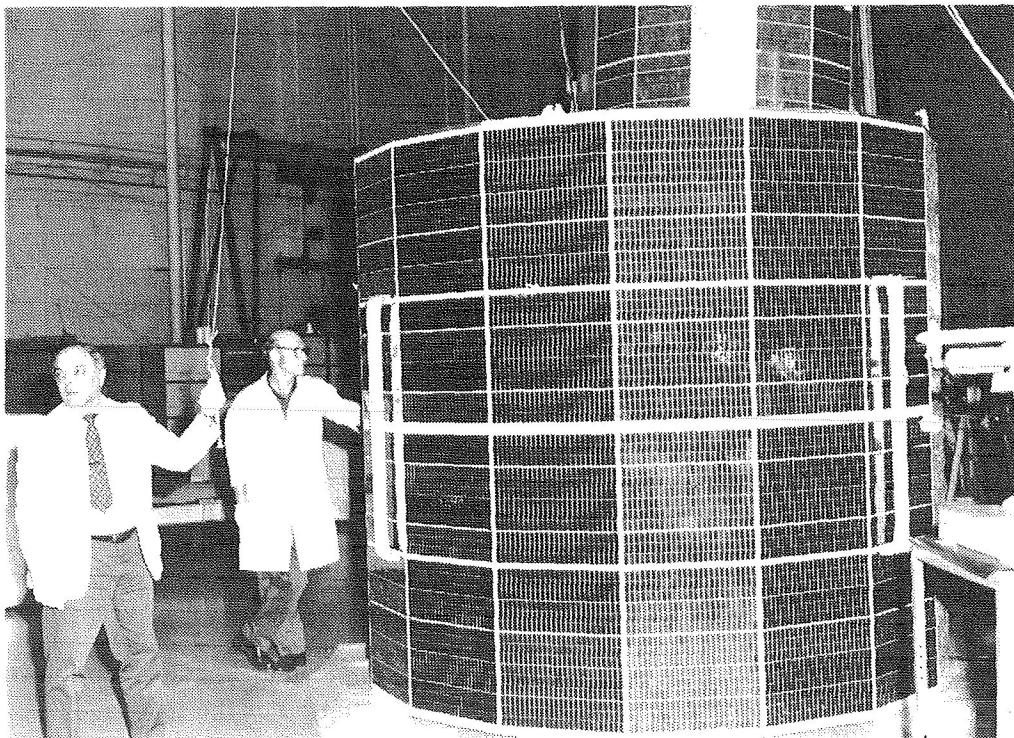


Figure 6. Solar array semicylinder.

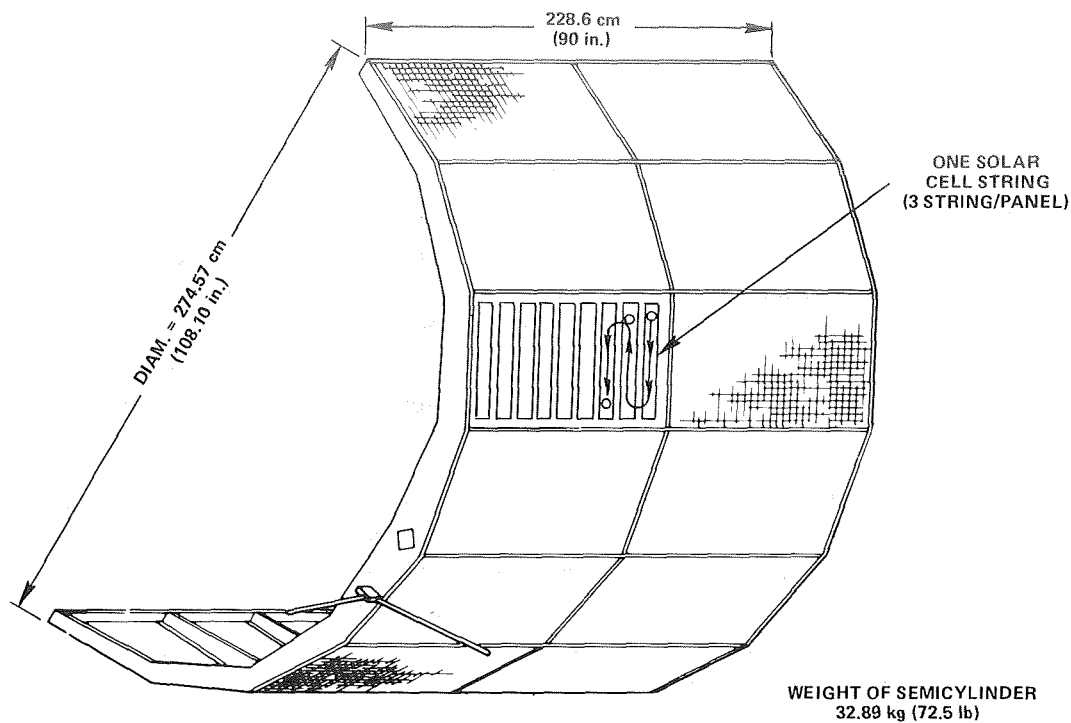


Figure 7. Solar array semicylinder showing a cell string.

Table 1
Electrical and Mechanical Panel Characteristics.

Mechanical Area	20 m ² (216 sq ft)
Solar Cell Area	17.3 m ² (186 sq ft)
Packaging Efficiency	86%
Number of Cells	675
Panel Weight	1.9 kg (4.18 lb)
Substrate Weight	0.98 kg (2.16 lb)
Power	70.5 W min @ 33.5 V, 28°C, AMO
Dimensions	118 cm (46.75 in.) by 55.4 cm (21.83 in.) by 1.9 cm (0.75 in.)

Design

The design of the solar array was dictated by the requirement to limit the degradation to less than 20 percent in two years. In addition to the consideration of the space radiation environment degrading the array, concern was also directed toward the degradation resulting from the extreme low temperature cycling. Because of the long eclipse periods (1.2 hours)

and the reduced effect of Earth albedo at synchronous altitudes, the low temperature limit for a conventional (rigid substrate) deployed solar array is significantly reduced from the typical low Earth orbit value of -80°C to -160°C . In addition, self-shadowing occurs on the arrays which induces additional thermal cycling even during the orbit when the spacecraft is in the Sun 100 percent of the time. This unique thermal cycling is shown in figure 8.

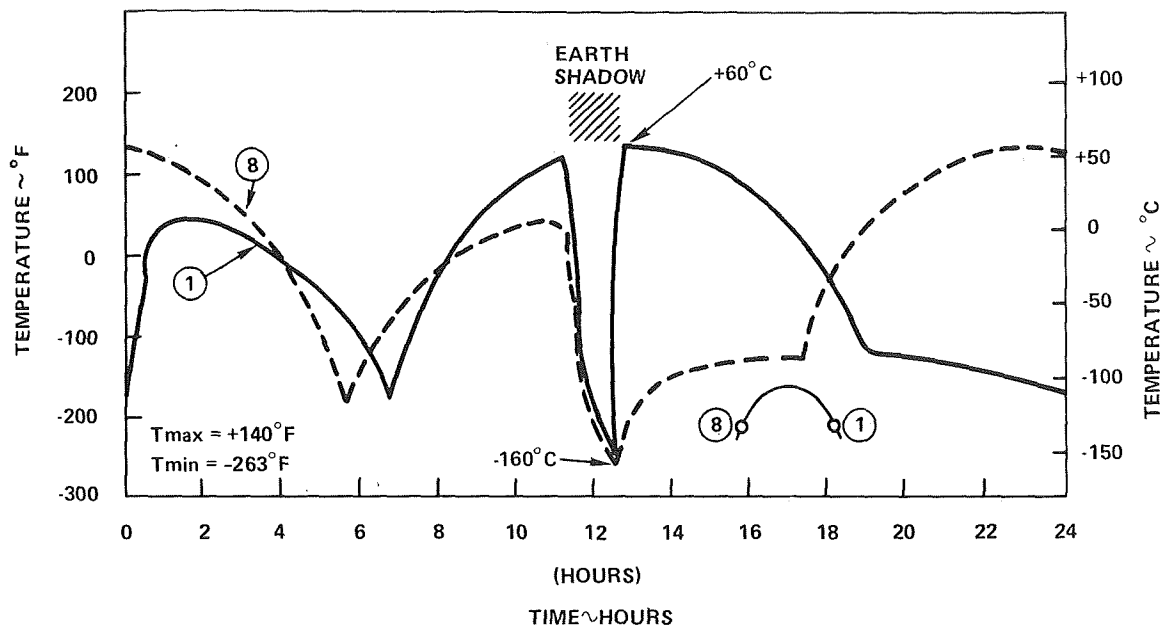


Figure 8. Solar panel temperature profile.

The solar cell interconnect selected to withstand this environment was 0.002-inch fine silver mesh. Three solder points are provided for each N (top) connection, and four solder points are provided for each P (bottom) connection. The solder tabs have small holes to enhance the flow of solder during the soldering process. The interconnect design included a very high stress relief loop to prevent the temperature extremes of $+60^{\circ}\text{C}$ to -160°C from stressing the solar cell contacts causing fatigue, wear, or breakage. In addition, the contacts have 90 percent solder fillets to minimize contact pull-away during thermal cycling.

Table 2 and figure 9 show the materials used in the buildup of the solar cell stack.

Test

With a well designed solar array, a major task was to incorporate a program into the spacecraft test flow that would minimize spacecraft test disruption while adequately testing the array. The large size of the array posed a significant challenge for testing the array while mounted on the spacecraft. In addition, test accuracy and repeatability were also important in order to analyze and evaluate the pretest and post-test data after each major spacecraft environmental test.

Table 2
Materials Used in the Solar Cell Stack.

Substrate	0.156 in. honeycomb with 5-mil Al faces
Substrate Insulation	2-mil Tedlar 200 BG 30 WH
Cell to Substrate Adhesive	Silastic 140, 50% coverage
Cover Glass Adhesive	Sylguard 182
Solar Cell	2 cm X 4 cm; 0.014 inch thick, 2 ohm cm, solder pressed Ti-Ag contacts
Solar Cell Interconnect	Stress relief loop, 0.002 inch photo-etched fine silver mesh
Cover Glass	6-mil Corning 0211 microsheet blue filter
Thermal Control Coating	MS-74 White Silicate Paint
Wire	Kapton Mil-W-81381/7B

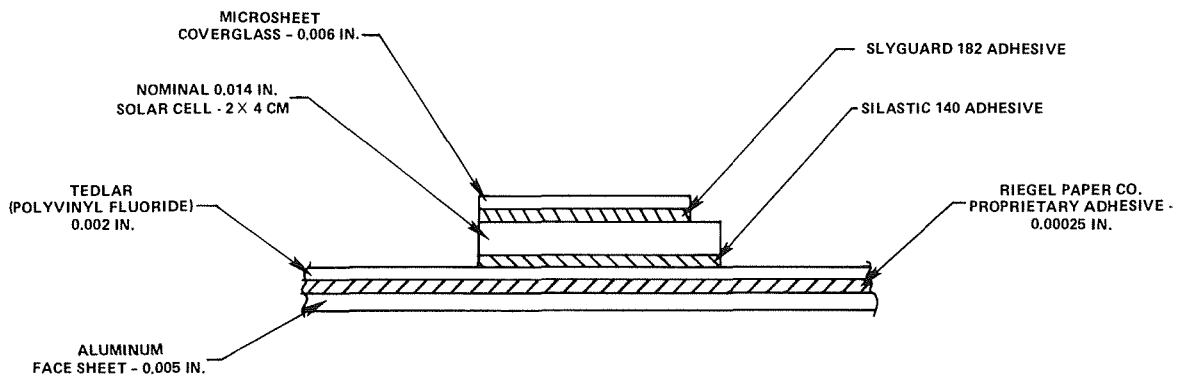


Figure 9. Solar cell stack.

The solar array test program was structured to provide the highest practical assurance that the solar array would meet its mission objectives. There were two levels of test. The first level was at the individual panel where thermal cycling of the panels was performed. This testing was performed to ensure that good quality panels were delivered to the spacecraft. The second level was at the spacecraft where a highly uniform air-mass zero flash illuminator was used to test each panel.

The prime driver behind the panel thermal cycling test was the extreme low-temperature limit of -160°C . (See figure 8.) A parametric thermal cycling test program was developed to determine the number of thermal cycles required to verify good hardware with the synchronous orbit temperature range. An inadequate number of thermal cycles might not sufficiently stress the hardware and, therefore, not expose manufacturing defects. An excessive number of cycles might reduce the life of the hardware.

The structure of the thermal cycle test program has to resolve this conflict by providing high confidence at minimum risk. The first step was to segregate a randomly selected lot of 40 panels (32 required for one spacecraft plus 8 spares) into 5 groups of panels each. The first group of 8 panels were subjected to 100 cycles from -160°C to $+60^{\circ}\text{C}$. Their I-V (current-voltage) curves were recorded and visual inspections made before and after the thermal cycling. These data were then used to compare to the second group which were subjected to 50 cycles and to the third group which were subjected to 25 cycles. Based upon this comparative analysis, all the remaining panels were then subjected to the minimum number of cycles required to ensure that most of the manufacturing defects would be detected and corrected. One of the conclusions drawn from the parametric thermal cycle test was that 25 cycles are sufficient to disclose workmanship defects with the synchronous orbit temperature range. Figure 10 shows the electrical performance as a function of cycles. As shown in this figure, a point was reached between 25 and 50 cycles where the degradation rate began to flatten out. Increased degradation would not be expected until the design-life point is reached and fatigue dominate the performance characteristics.

Comparison of the visual inspection data with the electrical data showed that the panels which experienced the greatest electrical degradation also had the largest number of mechanical defects. Within the 25- to 50-cycle range the panels with workmanship problems were effectively identified. A precision flash illumination system, the TRW large area pulse solar simulator (LAPSS), was used for testing the solar array at the panel string level while mounted on the spacecraft. The system consists of a pulsed 3-megawatt xenon flash unit and a temperature-intensity correcting data acquisition console. The data acquisition console automatically plots and prints on paper tape a ten point I-V curve from open-circuit voltage to short-circuit current with eight adjustable load points to show the I-V knee characteristics. The flash illumination uniformity was better than 1.0 percent over a target area of 0.74 m^2 (8 sq ft) and a distance between flash unit and panel of 9.1 m (30 ft).

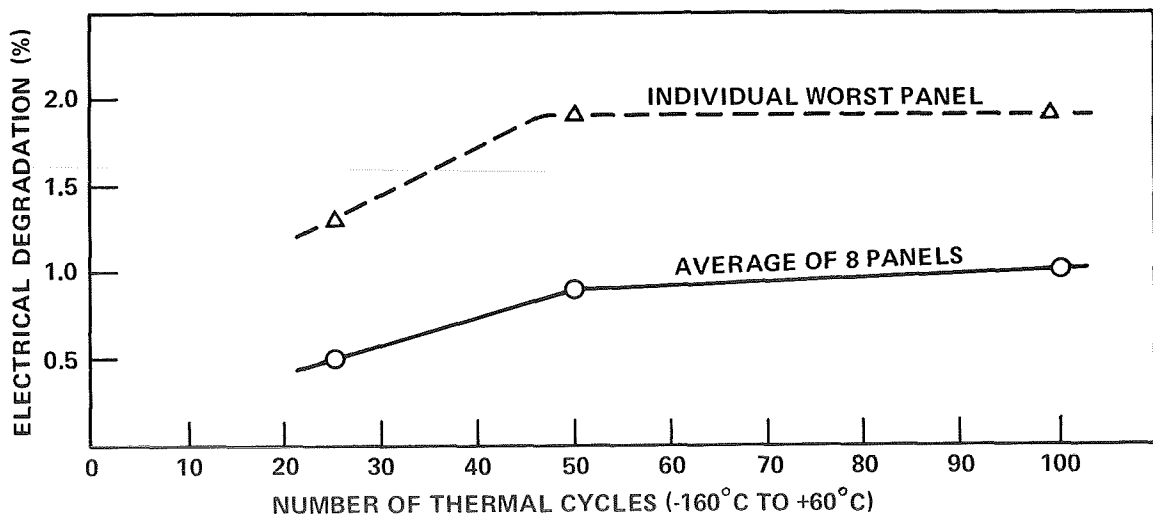


Figure 10. Panel electrical performance versus thermal vacuum cycles.

When tested on the spacecraft, the array was in the stowed position as shown in figure 11. Every panel and each string on every panel was tested by rotating the spacecraft 16 times on the Goerz table to place the panels under test normal to the illumination. The total time to completely check the I-V characteristics of all 32 panels, including setup, was approximately

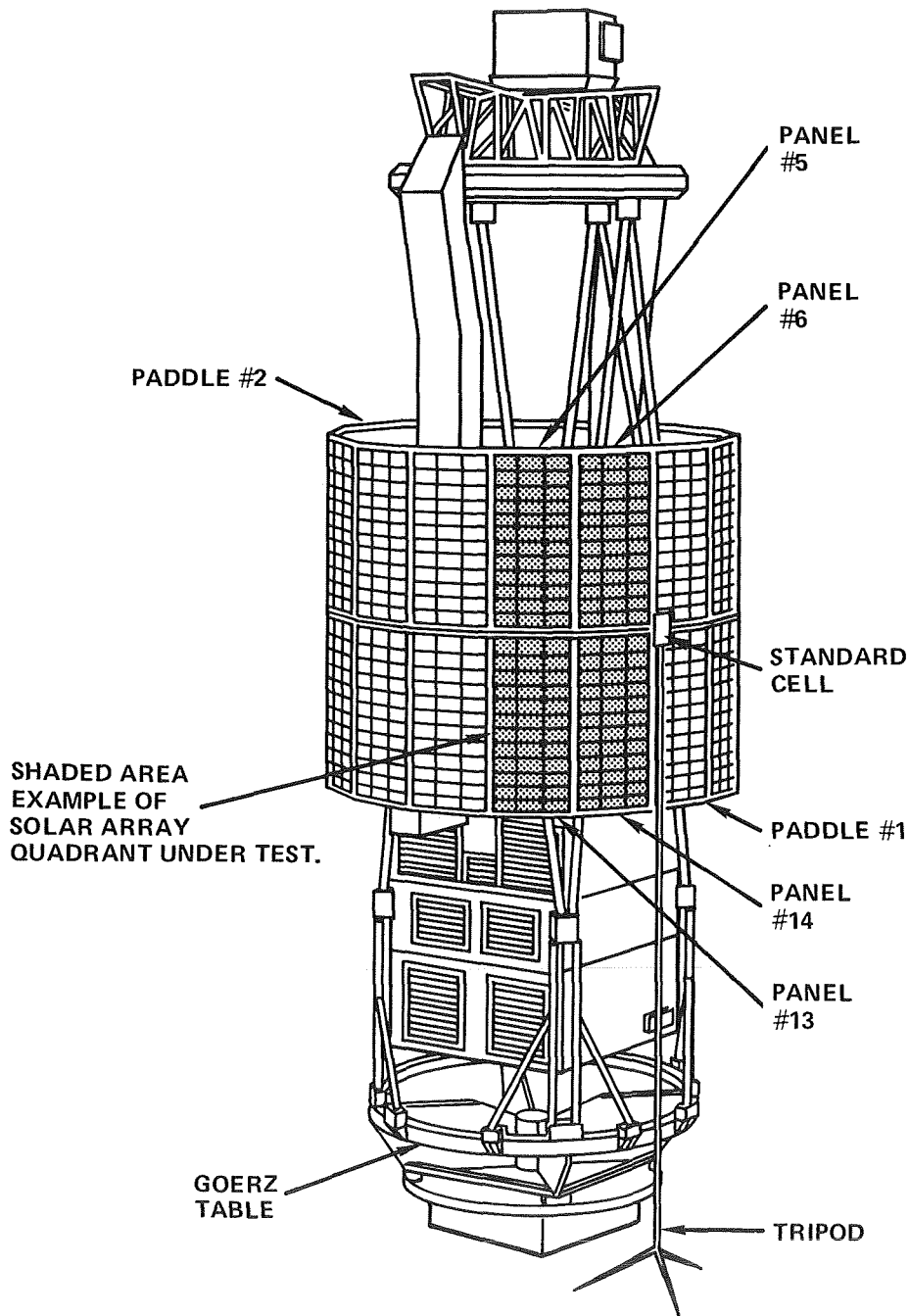


Figure 11. Test setup for solar array flash illumination.

4 hours. When the I-V characteristics of all 3 strings on each panel were taken and an I-V curve plotted for the panel itself, for a total of 128 I-V curves, the total test time was less than 12 hours. This technique minimized the interruptions to the spacecraft test flow.

Cleaning

Except for specific spacecraft tests, the array panels were covered for protection. After the solar panels had been on the spacecraft for several months, inspection showed that small amounts of film had collected on the surface of the coverslides. The presence of this film was of concern because, when exposed to ultraviolet radiation in space, the film could darken and cause a decrease of solar array power output (possibly as much as 5 percent); however, because of the large size of the array and the fragile nature of the high interconnects, serious consideration was given to the cleaning question. The first concern was to determine if there was sufficient film on the coverslide to warrant cleaning. Because of the accuracy and repeatability of solar testing with the flash illumination system, it was decided to clean and test the smallest testable unit on the array. Therefore, one series string (75 cells) on 3 separate panels was cleaned prior to shipment to the launch facility. An I-V curve (figure 12) was taken of each of the strings before and after cleaning. The data were consistent for all three strings. It showed that the film on the string of coverslides had reduced the string power output by 1.7 percent. Ultraviolet radiation in space could cause the film to darken and further reduce the power output; therefore, the decision was made to clean the panels at the launch facility. The panels were cleaned with trichlorethylene solution using cotton swabs and the total time required was 40 man-hours.

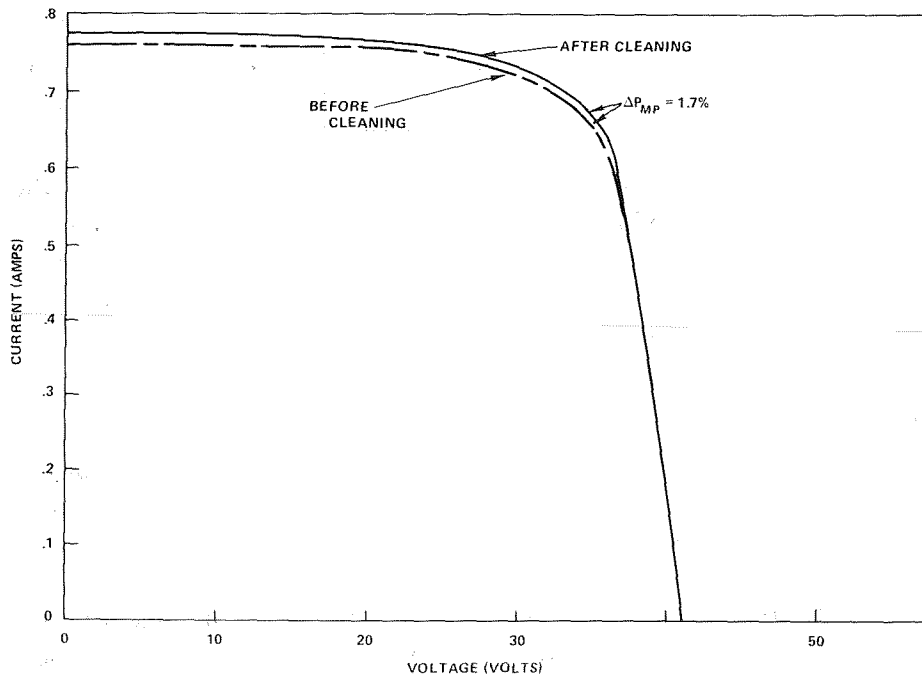


Figure 12. String I-V curve.

Electronics

Excluding the batteries and solar panels, the power subsystem consists of 21 separate electronics assemblies. Size, weight, and power handling capability of these units are given in table 3.

Table 3
 Sizes, Weights, and Power Handling Capability
 of Electronics Components.

Component	Qty	Size (cm)	Weight (kg)	Power Handling (per unit)
PRU	1	45.5 × 24.1 × 24.1	21.7	100 W (each redundant side)
LIC-15 W	1	12.7 × 8.9 × 10.2	0.92	15 W
LIC-60 W	1	12.7 × 8.9 × 10.2	0.96	60 W
LIC-92.5 W	2	12.7 × 8.9 × 10.2	1.02	92.5 W
LIC-150 W	2	12.7 × 8.9 × 10.2	1.02	150 W
LIC-35 W	1	12.7 × 8.9 × 10.2	1.0	35 W
PCU	1	30.5 × 29.7 × 17.8	7.2	1000 W (300 W redundant LICs)
Shunt Dissipator	12	12.7 × 8.9 × 6.3	0.61	35 W continuous, 50 W peak

Because of the large number of units, commonality of design was emphasized wherever practical to minimize cost and schedule risks and provide interchangeability where practical. For example, the 7 load interface circuits (LIC) vary in output power requirements from 15 watts to 150 watts; however, commonality among the low-level circuitry was used to minimize the number of electrical and mechanical designs.

Power Regulation Unit

The power regulation unit (PRU), the largest electronics box and the heart of the power subsystem, was laid out for ease in manufacturing. The PRU is composed of modules, printed circuit boards, hard-wired subassemblies, harnessing, and sheet metal brackets. The parts and subassemblies are housed in an aluminum dip-brazed container and mounted to attain thermal and structural integrity and maintain an orderly component location and circuit flow. All the low-level circuitry was placed on 21 plug-in printed circuit boards. The

heavy components, such as relays, inductors, and capacitors, were mounted on the internal walls of the container and the base plate. All high power dissipating components, such as transistors and diodes, were mounted on a heat sink below the printed circuit cards. This allowed uniform distribution of power throughout the box. The PRU is pictured in figure 13.

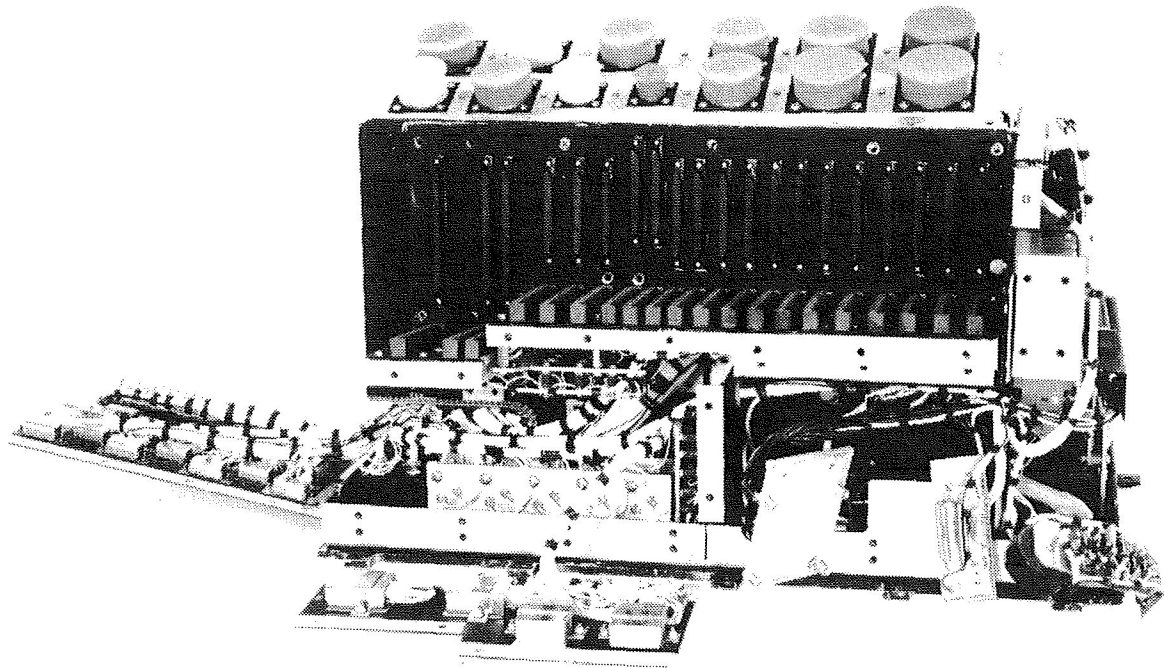


Figure 13. The power regulation unit.

Load Interface Circuits

The low-level circuitry (voltage sense, reference, error amplifier, current limit and drive electronics) is located on a printed circuit card that is identical for all units except for select-in-test components for output voltage and current limit setting. These cards are interchangeable and can be used for all LIC's. The output power stage consists of parallel power transistors mounted on heat sinks that are added as required to satisfy the output power requirements. The 150-watt LIC is pictured in figure 14.

Power Control Unit

The LIC commonality concept was carried over to the power control unit (PCU). The major portion of the PCU consists of two 300-watt LIC's and a host of signal conditioning circuitry for spacecraft temperature telemetry. The 300-watt LIC's in the PCU used the same printed circuit card as designed for the other LIC's. Changes were made only in the power handling circuitry and select-in-test components. The basic design of the PCU is similar to the PRU. The PCU is shown in figure 15.

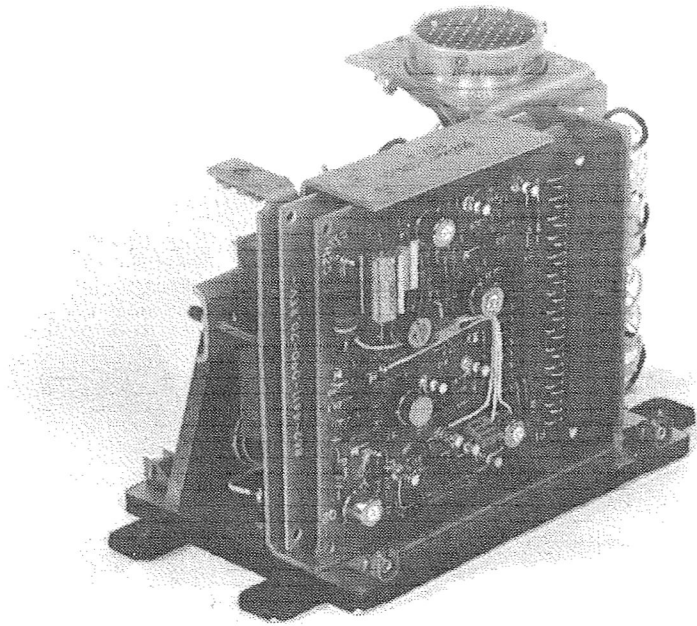


Figure 14. 150-watt load interface circuit.

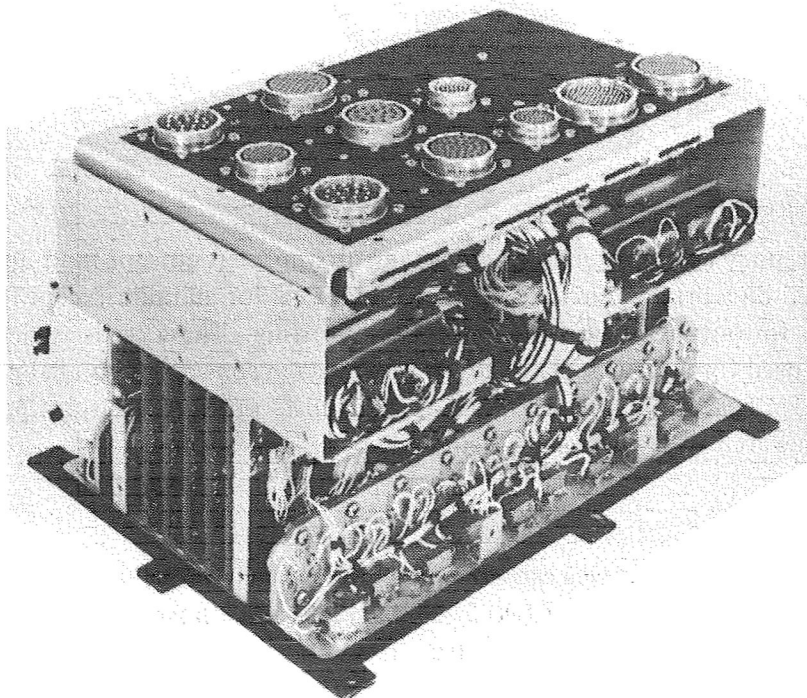


Figure 15. The power control unit.

Shunt Dissipators

There are 12 identical shunt dissipators that operate in conjunction with the PRU to regulate the spacecraft bus voltage. Each shunt dissipator is designed for a peak dissipation of 50 watts and a continuous dissipation of 35 watts. The peak dissipation of 50 watts occurred for several minutes during solar array deployment when both array semicylinders were illuminated by the Sun, thereby producing almost twice the normal array power.

The shunt dissipator functions by dissipating a portion of the energy produced by the solar array when the energy exceeds the spacecraft electrical load and battery charging requirements. Each shunt tap point is at two-thirds of the solar cell string length of 75 cells from the negative bus, thereby shunting 50 cells on each array (96 strings total with three 2 by 4 cm cells in parallel).

A shunt dissipator is shown in figure 16. The power dissipating components are mounted on heat sinks to provide good thermal transfer. With this design, the maximum junction temperatures of the power transistors do not exceed 115°C and 140°C respectively for the 35-watt continuous dissipation and the 50-watt peak dissipation.

The shunt dissipators are an integral part of the spacecraft thermal control system, and as such, it was important for the 12 units to share the power uniformly.

The unique solar array configuration using a semicylinder, consisting of panels subjected to different temperatures and angles of sunlight, made this more than a routine task.

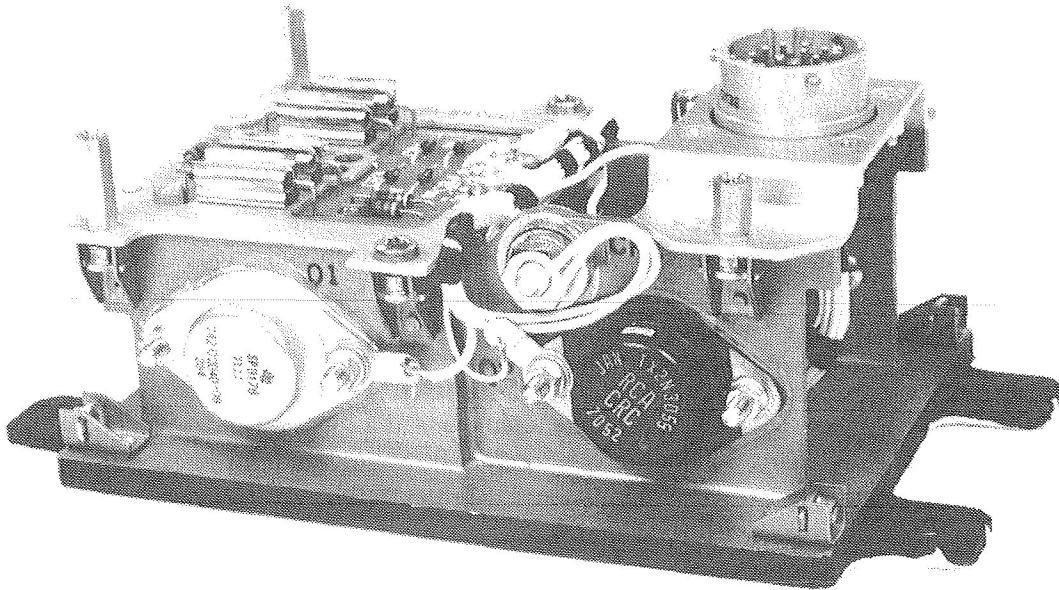


Figure 16. A shunt dissipator.

First, since all the shunts are driven from a common source, it was necessary to provide sufficient degeneration in the shunts to stabilize the transconductance gain ($\Delta I_o / \Delta V_{in}$) so that it would be predictable and well controlled. With stable gain, the output current drawn in all units, as a function of the input signal, would be the same. Test data of the transconductance gain of all 12 flight units shows that the variation in gain among all units is within ± 3 percent.

The next and most critical step was to provide a wiring matrix to the 3 tapped sections of each of the 32 panels so that the average voltage on all 12 shunts was approximately the same at any time throughout the spacecraft orbit.

In general, to provide power sharing for a partial shunt connected to a faceted array, each shunt should be connected to each facet. The ATS array has two panels per facet (shown in figure 7), totaling six strings per facet. The number of shunt dissipators, however, had been optimized at twelve. The practical configuration was to connect each shunt to one string on one panel on every other facet of the solar array. A total of eight strings is connected to each shunt as shown in figure 17. These connections, together with the stable transconductance of the shunts, allowed for uniform power dissipation.

Batteries

Two 19-cell, 15-ampere hour, nickel-cadmium batteries are used in the power system. The batteries are sized to provide sufficient power for the occult and load-share modes without exceeding a 50 percent depth-of-discharge (170 watt-hours per battery, 340 watt-hours total).

Each battery weighs 17 kg (37.5 lb) and is 23 cm (9 in.) long by 30.4 cm (12 in.) wide by 19 cm (7.5 in.) high. The cells are arranged in 3 rows of 7 cells per row with 2 rows each using a dummy cell. Each cell is separated from the adjacent cells by an L-shaped fin heat sink that is insulated with Kaptan tape. This configuration allows for each cell in each row to rest on a heat pipe for good thermal control. Three heat pipes, one per cell row, interface with the battery assembly. The battery is controlled to a temperature within 0°C to 25°C by the heat pipes and a louver assembly. Figure 18 is a photograph of the battery assembly. Note that the cells are held together by a skeleton frame open on all sides, top and bottom. After final assembly the exposed bottom section of the L fins are machined to provide a total base flatness of 0.001 inch. Each cell is hermetically sealed with dual ceramic-to-metal insulators isolating the terminals. The cases are 304 stainless steel, and each cell weighs 690 grams (1.52 lb) maximum. The cells were manufactured by Gulton Industries.

Three thermistors are incorporated into the heat sink fins at a location most responsive to battery cell temperature change. One thermistor is used for voltage-temperature compensation of the charger characteristic; the second is used in the battery overtemperature protection circuit, and the third is used for telemetry.

Three connectors are used with each battery. One connector provides the power interface to the power system while the second and third connectors are used for individual cell monitoring and ground test.

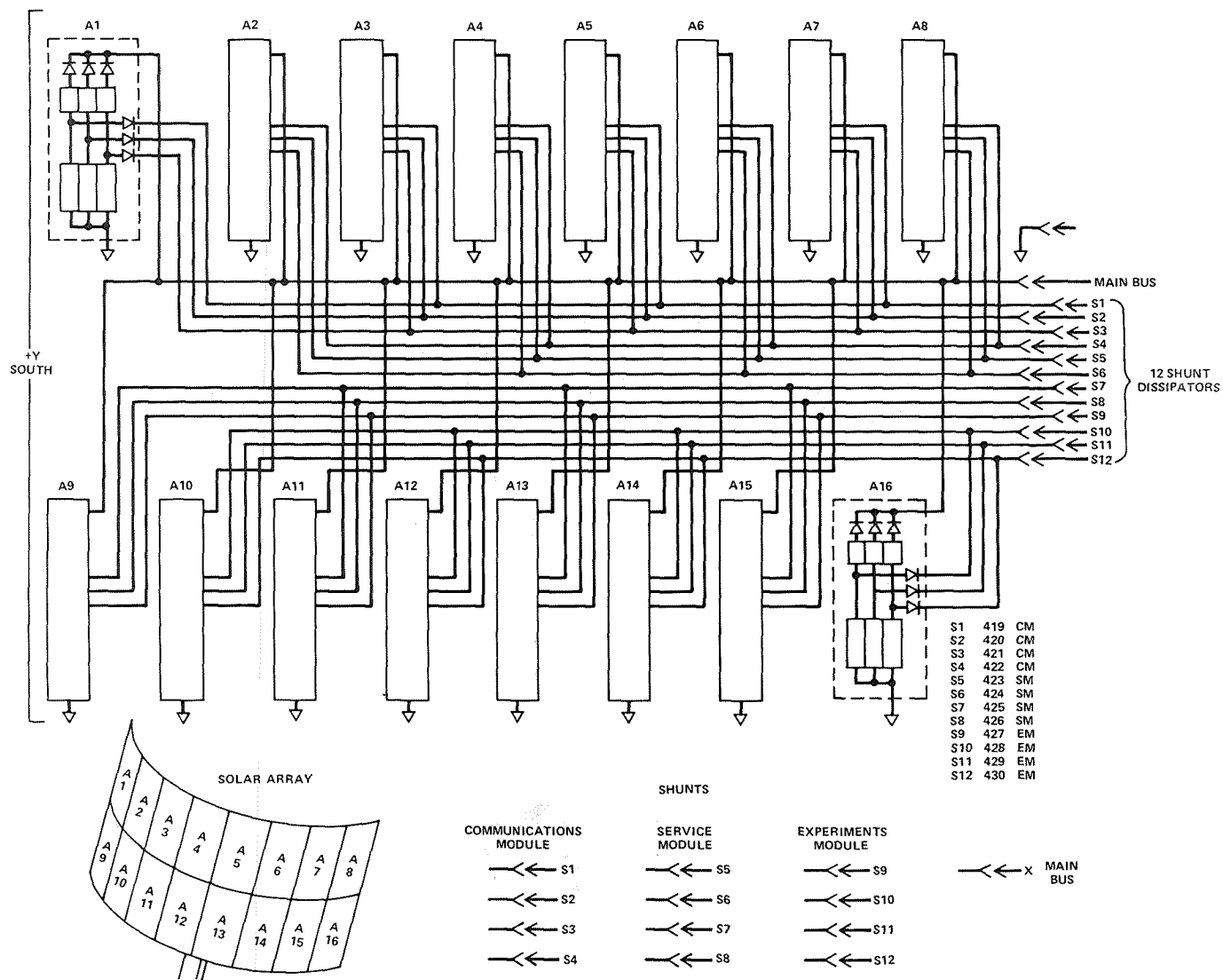


Figure 17. Solar array schematic diagram.

During the integration and ground testing of the spacecraft, test batteries were installed in place of the flight batteries to prevent degradation of the flight batteries due to uncontrolled charge and discharge cycling.

Following acceptance testing of the flight batteries, they were completely discharged, with each cell shorted, and stored in a controlled environment at 5°C. Just prior to the last spacecraft vibration test, which was the final test before shipment for launch, the flight batteries were reconditioned and installed in the spacecraft.

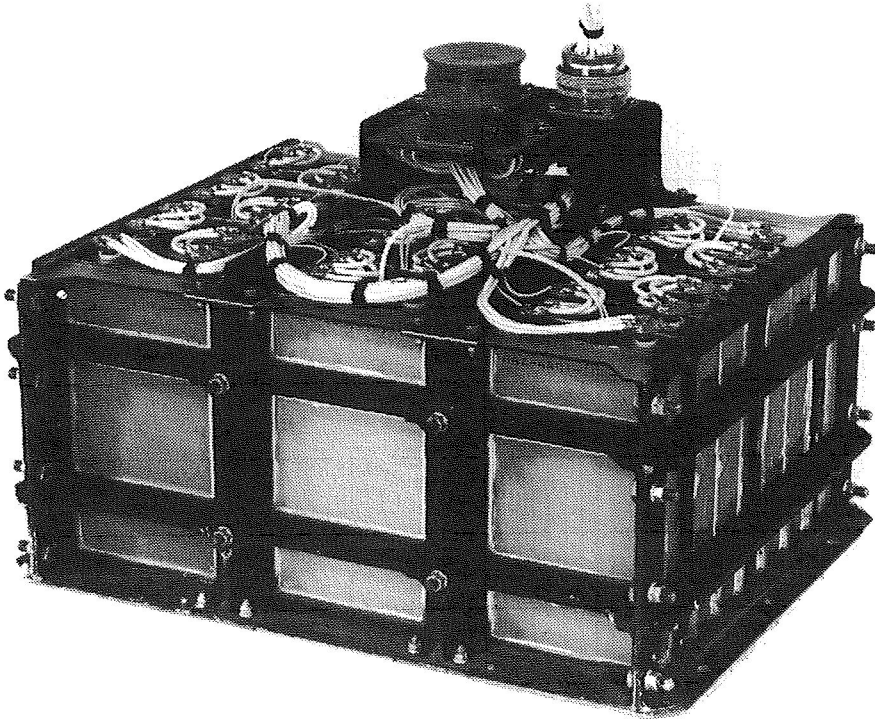


Figure 18. The battery assembly.

PERFORMANCE CHARACTERISTICS

Since all spacecraft subsystems interface at the power bus, it is here that subsystem interactions occur due to load current fluctuations and conducted electromagnetic interference. To minimize these interactions, it is important that the power system provide a low impedance bus with fast transient response.

The dynamic characteristics, as obtained by ground tests of the system, are described in the following paragraphs. For these tests, a solar array simulator was used to provide power to the power system. This simulator was designed to provide an I-V wave shape approximating the actual array characteristics including the tapped sections for the 12 shunt dissipators.

Dynamic Regulation

Table 4 shows the dynamic regulation requirements imposed on the power system.

The transient response of the power system to the instantaneous load change requirements is shown in the photographs of figures 19, 20, and 21. These figures demonstrate the regulation of the system in the shunt and boost modes. Also shown is the maximum voltage change that occurs for a load change which forces the system from shunt to boost mode and vice versa. For the response evaluation, a steady-state load of 7 amperes was applied to the system, while the dynamic load applied was a step of 8 amperes (240 watts), with rise and fall times less than 50 microseconds. The load varied from 7 amperes (210 watts) to 15 amperes (450 watts) and back to 7 amperes. The test was performed for 3 solar array power conditions, 500 watts, 400 watts, and 0 watts.

Table 4
Dynamic Regulation Requirements.

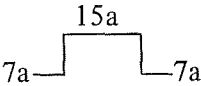
Load Current Change: 7 to 15 amp step wave with $t_{\text{rise}} = t_{\text{fall}} < 50 \mu\text{s}$, 	Maximum Voltage Overshoot	Maximum Voltage Undershoot	Maximum Response Time
a. $P_{\text{array}} = 500 \text{ W}$ b. $P_{\text{array}} = 400 \text{ W}$ c. $P_{\text{array}} = 0 \text{ W}$	3.05 V	3.05 V	2 ms

Figure 19 shows the bus response to the 500-watt array condition. Since the array capability exceeds the maximum load of 450 watts, this test demonstrates the response of the shunt mode including the effects of the long 10-meter (35-ft) array harness. Note from this figure that the application of the 8-ampere load resulted in an undershoot of 0.3 volt with recovery back to steady state in 0.6 milliseconds (ms). The removal of the 8-ampere load resulted in an overshoot of 0.32 volt with recovery in 0.6 ms.

Figure 20 shows the bus response to the 400-watt array condition. For this test, the dynamic load requirements of 450 watts (15 amperes) exceeds the capability of the array and the boost regulator must turn on and supply the additional power. This test shows the worst case voltage change on the bus, from shunt through charge to boost mode and back to shunt.

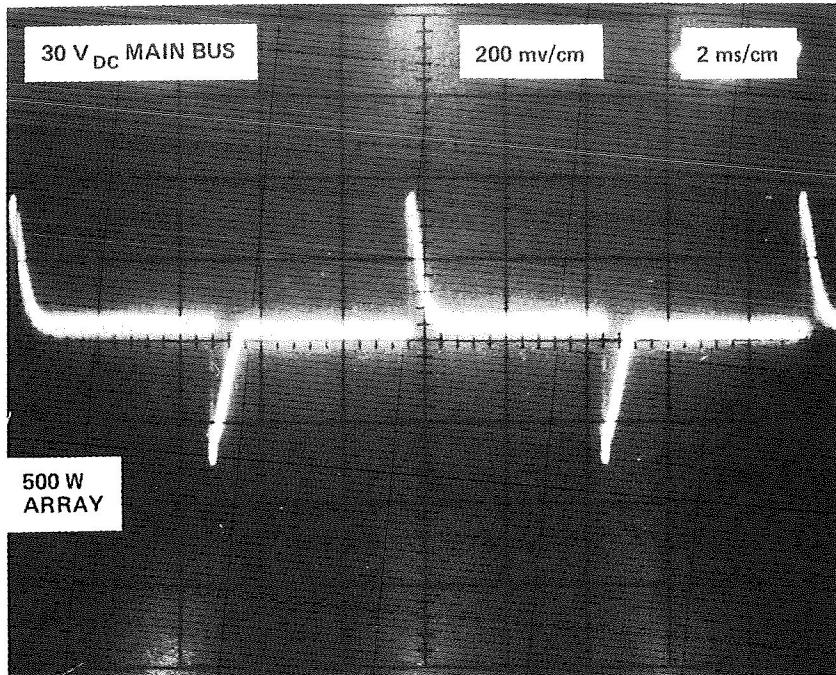


Figure 19. Dynamic regulation (shunt mode) 500-watt solar array.

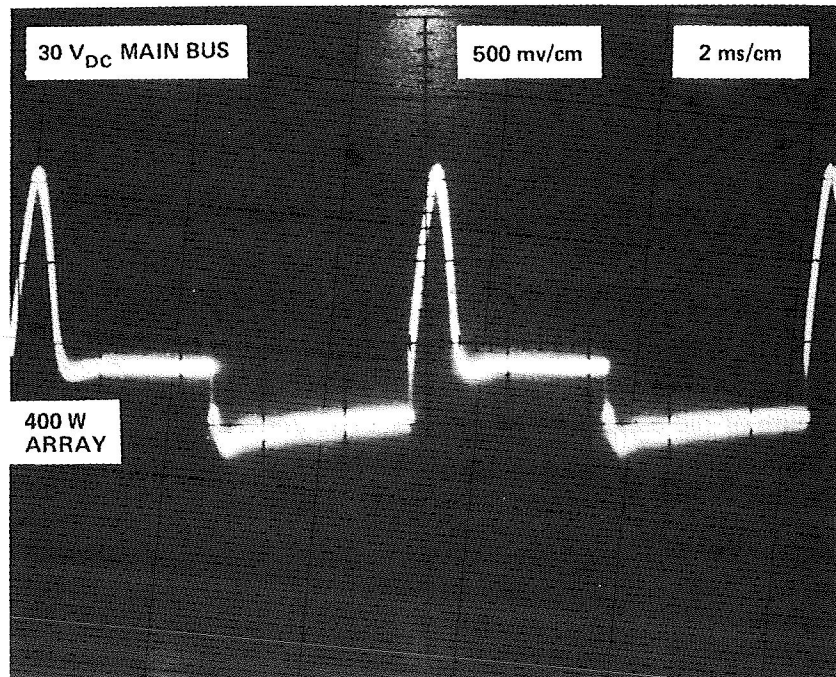


Figure 20. Dynamic regulation (shunt/boost mode) with 400-watt solar array.

The application of the 8-ampere load did not result in any undershoot. The change in steady-state value is due to the 0.15-volt deadband separating the boost mode from the charge and shunt modes. The overshoot that occurred on removal of the 8-ampere load was 1.4 volts with recovery in 1.2 ms.

Figure 21 shows the bus response to a zero-watt array. For this condition, only the boost mode is active with the battery supplying the load through the boost regulator. The application of the 8-ampere load resulted in an undershoot of 0.66 volt with recovery in 0.6 ms. An overshoot of 0.9 volt with recovery within 0.6 ms resulted from the removal of the 8-ampere load.

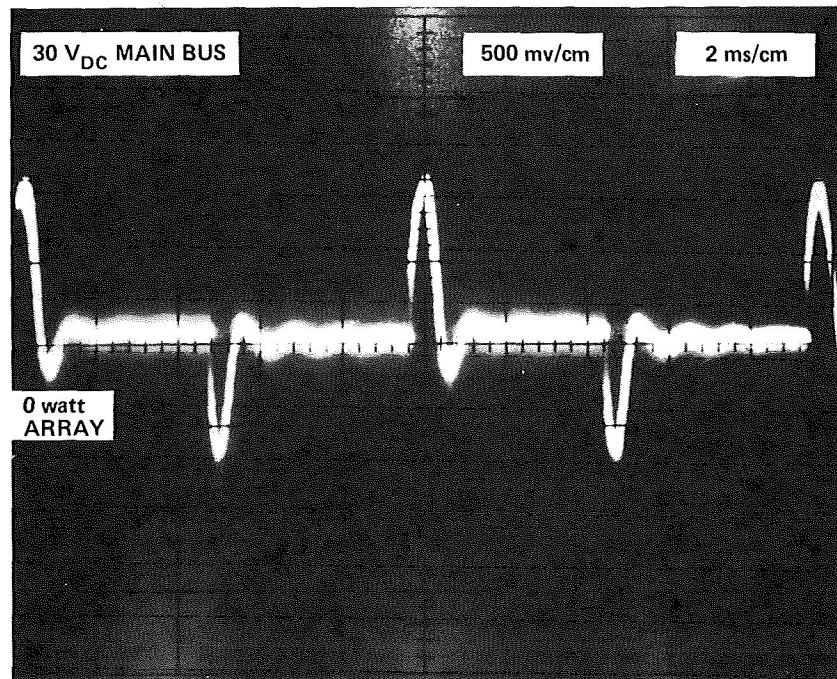


Figure 21. Dynamic regulation (boost mode) with 0-watt solar array.

These figures show the excellent dynamic regulation and transient response of the ATS-6 system. This performance was achieved by providing fast responding feedback loops in the shunt, charge and boost modes. Gain crossover for the shunt loop was set at 20 kHz, the charge-loop crossover was set at 5 kHz, while the boost-loop crossover was 2 kHz. In addition, the linear shunt circuit configuration and the autotransformer boost circuit also provide fast response to the feedback error signals. Since the shunt and boost regulator designs and the feedback bandwidths provide excellent response, the main bus capacitors needed for

energy storage could be minimized. Only 2000 microfarads of capacitance was used resulting in a substantial reduction of weight and volume.

With this capacitance and regulation, a maximum of 50 millivolts of ripple voltage occurs on the main bus in the boost mode (eclipse operation). That compares to a specification maximum of 150 millivolts. In the shunt mode, (operation in sunlight), where the system operates most of the time, a ripple voltage of less than 10 millivolts occurs.

Output Impedance

The output impedance of the power system is shown in figure 22 for the primary modes of operation—the shunt and boost. The impedance for both modes is quite low—well below 0.1 ohm which accounts for the excellent dynamic performance. A close look at the curves shows that the maximum impedance of 0.06 ohm occurs at about 2 kHz, the 0 dB gain crossover for the boost feedback loop. For the shunt mode, which has higher loop gain and bandwidth, a maximum impedance of 0.035 ohm occurs.

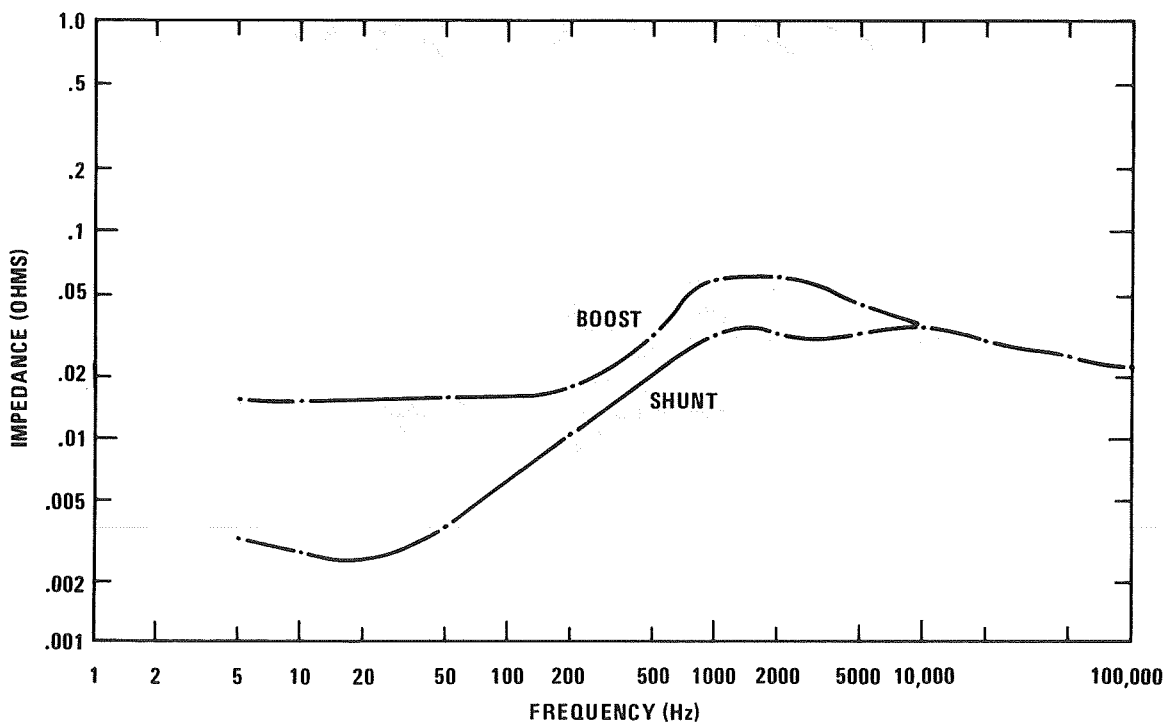


Figure 22. Output impedance.

Overload Protection

To protect the spacecraft subsystems from bus transients due to the occurrence of an overload or short in any load, a unique protection system was incorporated into the power system. If an overload (over 1100 watts in sunlight and 500 watts in occult) occurred, the boost regulator cycles off for 90 ms and linearly on for 10 ms to sample for presence of the overload. During the 90 ms that the boost regulator is off, the bus is clamped to the battery. If the overload continues for 250 ms, the nonessential relay will open disconnecting the nonessential loads. Should the overload remain, the regulator will continue to cycle on and off linearly until an additional 250 ms has elapsed. At that time the power system is automatically reconfigured to its standby redundant units. Should the overload or fault continue, it will be cleared by the battery since the battery is applied directly to the regulated bus to provide a high current source for clearing faults. Figure 23 shows the PRU and PCU fault signals generated to control removal of nonessential loads and switchover to the standby redundant units.

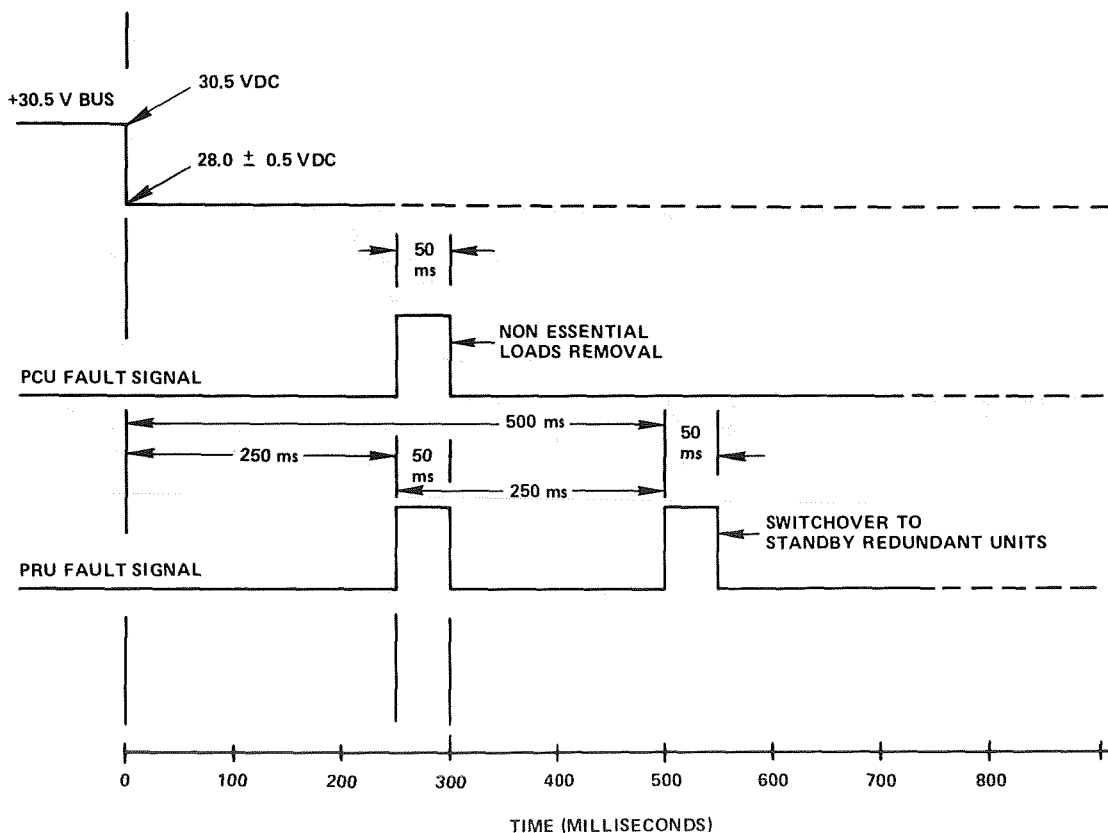


Figure 23. PCU timing scheme for bus protection.

Figures 24 and 25 show the actual performance of the power system to both nonessential and essential bus faults. Note the smooth linear rise and fall of the bus voltage and the absence of any fast bus voltage transients. In figure 24, the opening of the nonessential bus relay removed the overload and the bus voltage smoothly recovered to the regulated level of 30.5 Vdc. Transfer to the standby regulation units did not occur as evidenced by the absence of a 5-volt level change in TP39 (telemetry signal indicating on/off status of redundant units in the PRU). In figure 25, the overload was removed after 650 ms. For transfer to standby units, 500 ms is required. The change of 5 volts in the level of TP39 shows the transfer of the system to the redundant units. A smooth voltage recovery is again evidenced.

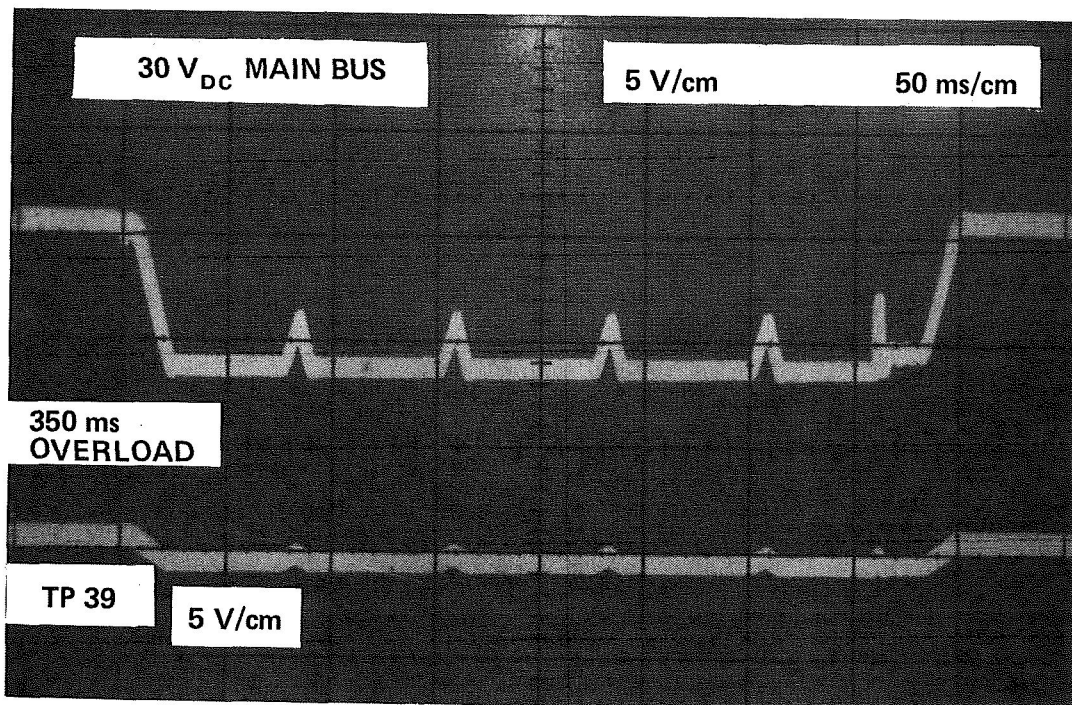


Figure 24. Bus response to nonessential bus overload.

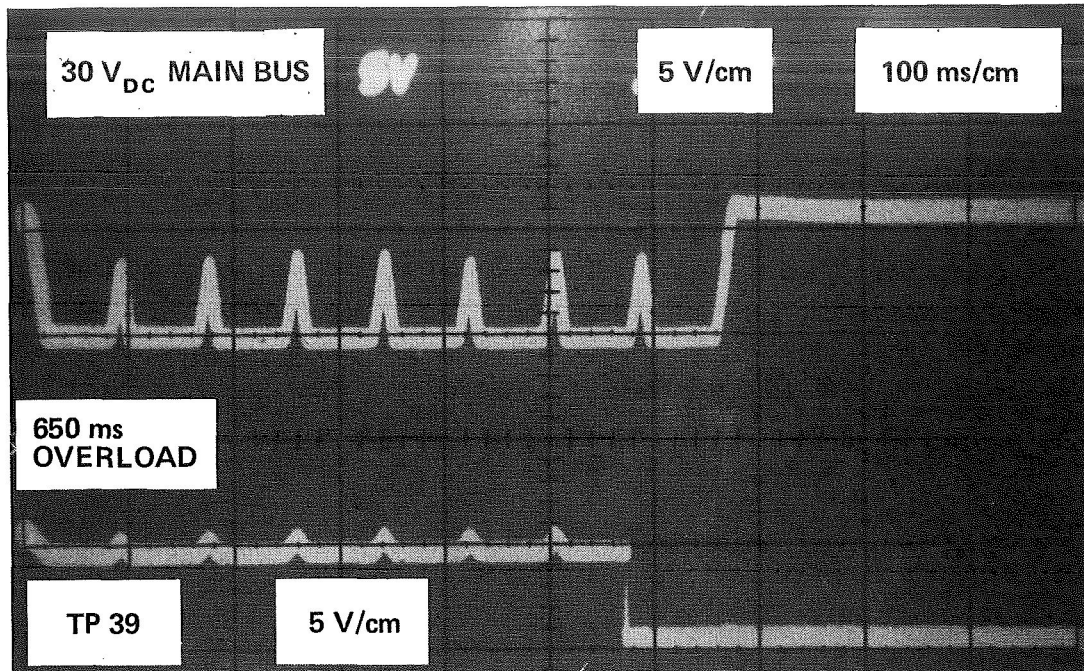


Figure 25. Bus response to essential bus overload.

Load Interface Circuits

The load interface circuits (LIC) are incorporated in the power system to control the interface between the 30.5-volt bus and the GFE experiment loads. To control this interface, the LIC's provide the following major functions:

- Provides regulated dc voltage ($28\text{ V} \pm 2\%$) to load under varying input and load conditions.
- Protects power system from malfunction, if the load should short, by acting as an electronic fuse.
- Provides on-off power switching to load through ground command.
- Provides undervoltage protection for load by automatically removing power from load if the power system output voltage drops to low level.
- Isolates load from ripple voltage and noise on input voltage to LIC.
- Provides a low impedance bus to the loads.

The I-V characteristic of the output of each LIC is shown in figure 26. This characteristic shows the voltage regulation mode, constant current mode for overload protection, and undervoltage protection mode.

Line isolation of noise and ripple voltage is provided by the ability of the LIC's to attenuate input variations over a broad frequency range. Input ripple rejection as a function of frequency for a 300-watt LIC is shown in figure 27.

Output impedance characteristic of a 300-watt LIC is shown in figure 28.

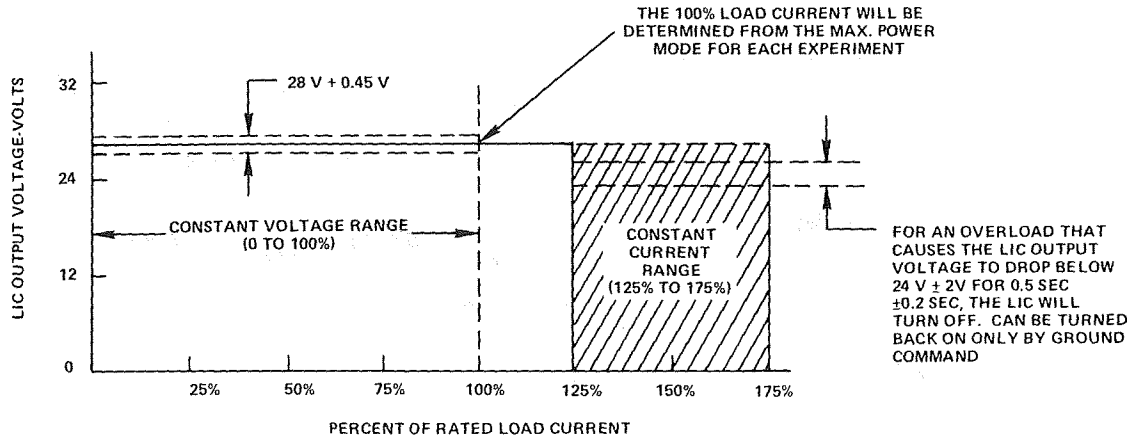


Figure 26. Regulation characteristics of the LIC.

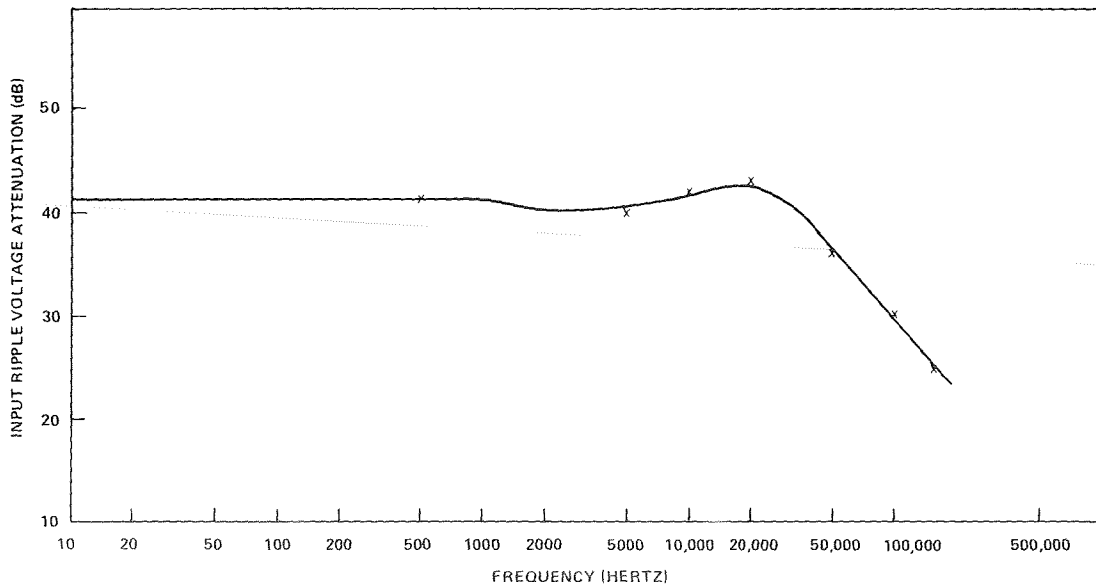


Figure 27. LIC input ripple voltage attenuation vs frequency.

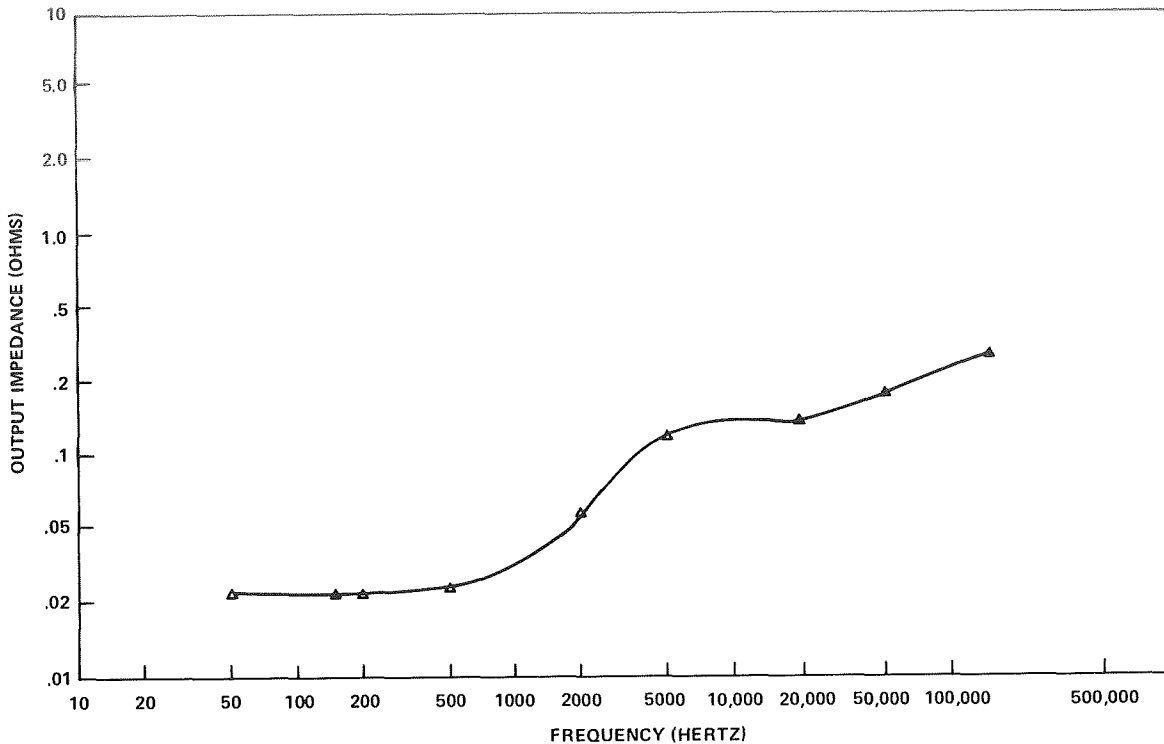


Figure 28. Load interface circuit output impedance.

ORBITAL PERFORMANCE

Solar Array

The solar array performance in orbit is a function of radiation damage, thermal cycling effects, the season of the year, and the pointing maneuvers required in orbit. At any given time, the power output is maximum at the equinox and minimum at summer solstice, due to the effect of Earth-Sun distance and the angle of solar incidence. The array temperature profile has been as predicted. The severe temperature extremes of -160°C to $+60^{\circ}\text{C}$ occurred during the eclipse seasons, and no unexpected degradation of the array has occurred due to this thermal cycling. This thermal cycling has, however, caused the loss of two of the four temperature sensors mounted on the back of the array.

The power output of the solar array during the first two years in orbit is shown in figure 29. As can be seen by this figure, the actual array power has tracked the predicted array power remarkably well. An average degradation of 18.5 percent has occurred after 2 years compared to 20 percent predicted. After nearly 3 years in orbit, a degradation of 19.2 percent has occurred versus 22 percent predicted. The level shown is the power available at the terminals of the power regulation unit, accounting for isolation-diode and harness resistance losses.

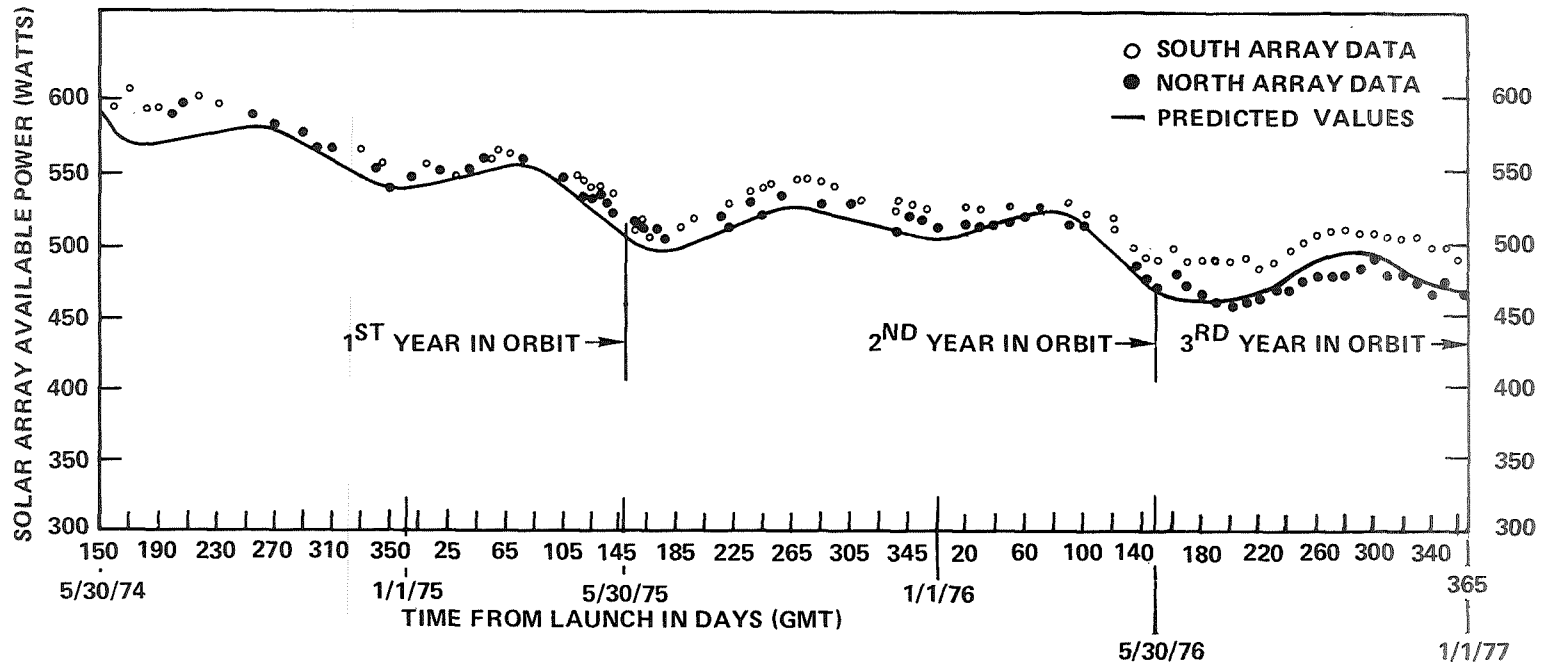


Figure 29. Measured solar array power.

Since the array is composed of two semicylinders that behave as a cylinder with displaced halves that rotate once a day, a relatively constant solar array power is provided throughout the orbit. All the data for the figure, however, were taken at 6 a.m. and 6 p.m. (spacecraft time) when only the south or north array is illuminated. This allowed the evaluation of array power out of each array half (each semicylinder). As shown, both array halves are performing as predicted. The north array has experienced slightly more degradation than the south array with the south array delivering about 30 watts more than the north array.

The yearly seasonal variations are apparent in the figure. The maxima occur at the equinox, and the deep minima at summer solstice. The intermediate minima occur at winter solstice, when the solar constant is about 7 percent higher than at summer solstice.

Electronics

Since spacecraft launch on May 30, 1974, the power system electronics have performed well within the specifications, fully satisfying the design requirements. Although redundancy is incorporated in the power system electronics to avoid single point failures, switchover to a redundant unit has only been necessary for flexibility in battery charging.

Table 5 is a specification compliance matrix showing the performance of the major parameters and components of the power system.

Power Control Unit (PCU) and Load Interface Circuits (LIC)

The performance of the PCU and the LIC's have been well within specifications. Table 5 shows the performance of the regulated bus voltages of these circuits.

Power Regulation Unit

The performance of the power regulation unit (the heart of electrical power system) has been monitored in its major operating modes. These major modes of operation are shown in figure 30 which is a typical plot of the static load performance of the power system bus. The telemetered data shown were taken with the system in the boost mode, boost/charge deadband, charge mode, and shunt mode. The beginning of life bus I-V curve is also shown on this figure. The entire regulation occurs within a band of 30.2 V to 30.6 V (ΔV of 0.4 V) which is well within the bus specification of 30.5 Vdc $\pm 2\%$ (ΔV of 1.22 V). In addition, there are no indications of overlapping modes or excessive spreads in the deadbands, since the modes of operation are close to the predicted voltages.

A photo of the preflight main bus excursion through the three modes—shunt, charge, and boost—is shown in figure 31. Note that the deadband between shunt and charge is 30 millivolts and between charge and boost is 150 millivolts.

Table 5
Electrical Power System: In-Orbit Performance

Component/Parameter	Specification	In-Orbit Performance
Spacecraft Bus Voltage	+30.5 V \pm 2%	+30.5 V $\begin{matrix} +0.3\% \\ -0.9\% \end{matrix}$
Battery 1 Charge Current Limit	1.5 A $\begin{matrix} +0.15 \text{ A} \\ -0.08 \text{ A} \end{matrix}$	1.5 A $\begin{matrix} +0 \text{ A} \\ -0.03 \text{ A} \end{matrix}$
Battery 2 Charge Current Limit	1.5 A $\begin{matrix} +0.15 \text{ A} \\ -0.08 \text{ A} \end{matrix}$	1.5 A $\begin{matrix} +0 \text{ A} \\ -0.03 \text{ A} \end{matrix}$
Battery 1 V/Temp	26.88 V \pm 0.2 V @ 17.4°C	26.9 V @ 17.4°C
Battery 1 Charge Taper Performance	26.58 V \pm 0.2 V @ 22.8°C	26.6 V @ 22.8°C
Battery 2 V/Temp	26.88 V \pm 0.2 V @ 17.4°C	26.8 V @ 17.4°C
Battery 2 Charge Taper Performance	26.58 V \pm 0.2 V @ 22.8°C	26.5 V @ 22.8°C
LIC (QCM)	28.0 V \pm 0.45 V	27.9 V
LIC (VHRR)	28.0 V \pm 0.45 V	28.0 V
LIC (MMW 1)	28.0 V \pm 0.45 V	27.9 V
LIC (MMW 2)	28.0 V \pm 0.45 V	27.9 V
LIC (PROP)	28.0 V \pm 0.45 V	28.0 V
LIC (ION 1)	28.0 V \pm 0.45 V	28.1 V
LIC (ION 2)	28.0 V \pm 0.45 V	28.0 V
PCU Regulator 1	28.0 V \pm 0.45 V	28.1 V
PCU Regulator 2	28.0 V \pm 0.45 V	28.2 V
PCU LIC (EME)	28.0 V \pm 0.45 V	28.0 V

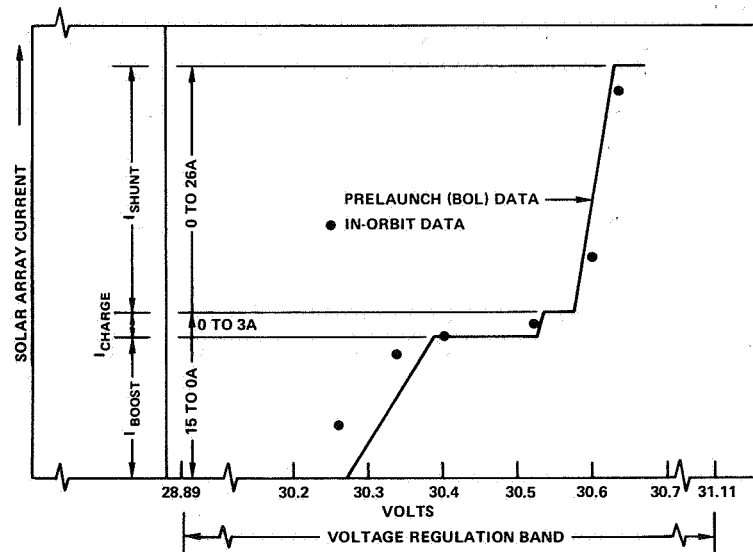


Figure 30. Regulated bus data.

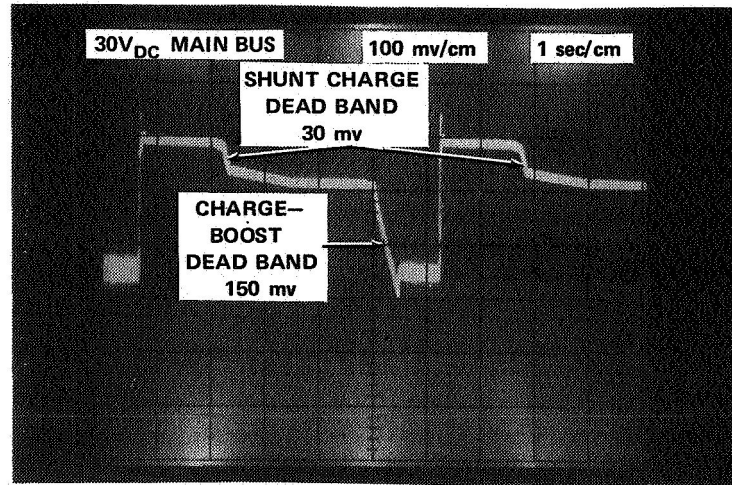


Figure 31. Preflight deadbands.

Shunt Dissipators

Table 6 shows how uniformly the 12 partial shunt dissipators have shared the excess solar array power. Two cases are tabulated: (1) low shunt dissipator power ($I_{sh} = 1.7$ amp) and (2) medium shunt dissipator power ($I_{sh} = 10.4$ amp). Since total shunt dissipator current is telemetered, instead of each of the 12 individual shunt currents, the assumption is made that each shunt current is 1/12 of the total. This is reasonable since the ground test data on all the shunt dissipators showed close current sharing. The tap voltages shown in table 6 are telemetered data.

Battery Performance

The ATS-6 mission has resulted in a unique battery cycling regime for synchronous orbit. The batteries have been discharged to varying depths from 5 percent to 60 percent daily. In addition, during the second year, discharges have occurred twice a day to depths up to 35 percent and 45 percent respectively. Normally for synchronous orbit, the batteries are required to support the spacecraft during the eclipse seasons only. However, on ATS-6, an early decision was made to use battery power to supplement the array for peak loads rather than increase the array size and weight. This decision was also based on the fact that the power system design would provide the highest overall system efficiency by forcing the array to supply all available power and requiring that the battery supply only the deficiency.

Daily battery discharge cycles have occurred during the first and second years and part of the third year of operation. Table 7 shows the number of discharge cycles versus the depths of discharge (DOD) range for nearly three years of operation including six eclipse periods.

Table 6
Shunt Dissipator Power Sharing

Shunt Dissipator	GMT 190:02:13 $I_{SA} = 17.8 \text{ A}$ $I_{SHUNT} = 1.7 \text{ A}$			GMT 151:22:33 $I_{SA} = 10.2 \text{ A}$ $I_{SHUNT} = 10.4 \text{ A}$		
	Tap Voltage	Dissipator Current	Diss. Power	Tap Voltage	Dissipator Current	Diss. Power
A419	19.2	0.14 A	2.68 W	17.2	0.9 A	15.5 W
A420	19.6	↓	2.74 W	17.6	↓	15.8 W
A421	19.3		2.7 W	16.9		15.2 W
A422	19.1		2.67 W	16.8		15.1 W
A423	19.3		2.7 W	16.9		15.2 W
A424	19.9		2.79 W	16.7		15.0 W
A425	18.8		2.63 W	16.8		15.1 W
A426	19.5		2.73 W	17.5		15.8 W
A427	19.1		2.67 W	16.9		15.2 W
A428	19.7		2.76 W	16.7		15.0 W
A429	19.5		2.73 W	17.5		15.8 W
A430	19.2		2.68 W	16.9		15.2 W

The second year of operation subjected the batteries to greater depths of discharges and more frequent discharge cycles than had been previously planned. In the second year, for example, the Satellite Instructional Television Experiment (SITE) to India was operated twice a day. During this operation, the combination of experiment loading combined with the SITE operation has exceeded the power out of the array requiring the battery to provide the additional load power. The battery discharge profile for SITE operations is shown in figure 32. Note that twice daily discharges of 35 percent and 45 percent DOD during the noneclipse season have been routine. During the eclipse seasons, discharges three times a day have occurred; the eclipse discharge (peak of 50 percent DOD) and the two SITE discharges (reduced to 15 percent and 25 percent DOD).

Note from table 7 the dramatic increase in the number of discharges in the 20 to 30 percent and 30 to 40 percent ranges caused by SITE operations. Also note that of the 1401 total discharge cycles, 1013 have been at depths of greater than 20 percent. Also of the 1401 cycles, 1137 have been noneclipse discharges.

For the eclipse discharge, figure 33 shows the discharge characteristics for eclipse seasons 1 through 6 for the maximum shadow of 72 minutes.

Table 7
Battery Discharge Cycles

Depth of Discharge	No. of Discharge Cycles			Total Number Cycles May 30, 1974 to April 12, 1977
	May 30, 1974 to July 1, 1975	July 1, 1975 to August 19, 1976 (SITE Operation Period)	August 19, 1976 to April 12, 1977	
5 to 10%	102	5	31	138
10 to 20%	129	90	31	250
20 to 30%	68	324	26	418
30 to 40%	54	324	37	415
40 to 50%	54	91	24	169
50 to 60%	5	2	0	7
80 to 90%	0	3	1	4
Total	412	839	150	1401
Eclipse Cycles	88	88	88	264
Noneclipse Cycles	324	751	62	1137

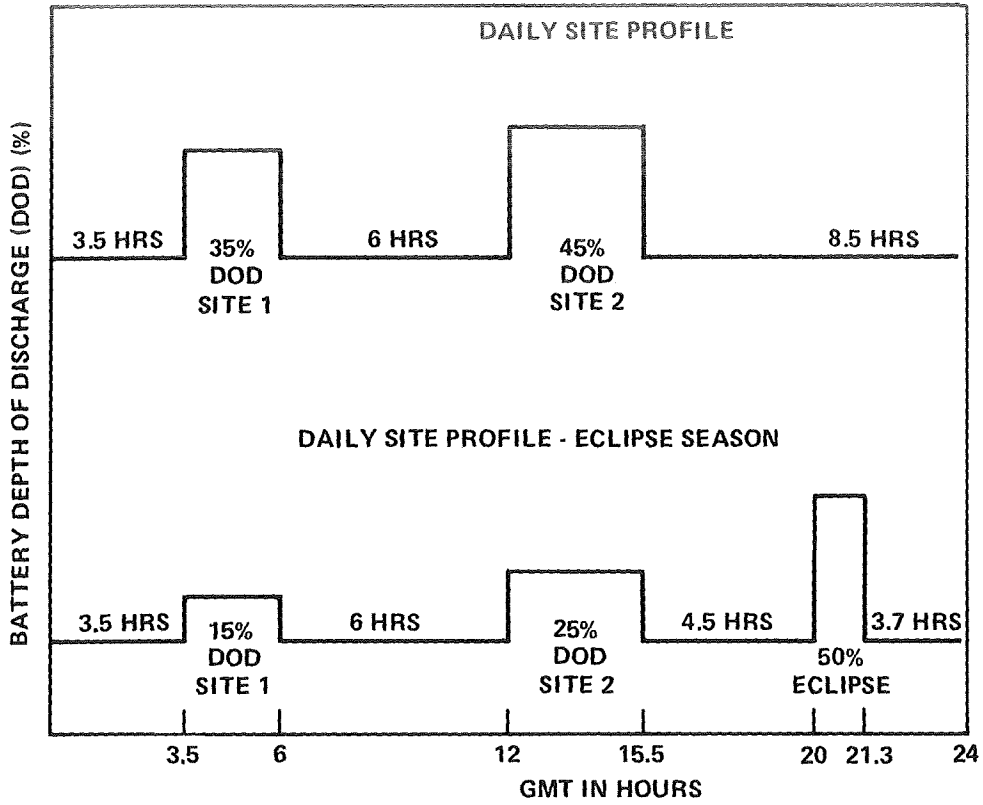


Figure 32. Battery discharge profile for SITE operations.

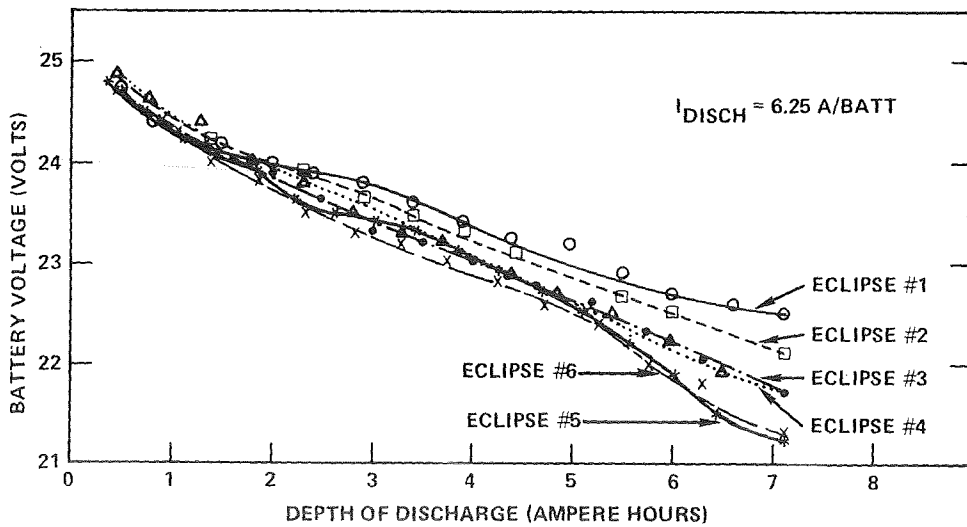


Figure 33. Battery discharge curves for eclipse seasons #1 through #6.

The end-of-discharge (EOD) voltage for eclipse season 3 appears to be lower than expected. The reason for this was found to be insufficient battery charging. This problem was discovered after the third eclipse during SITE. It was noted that the EOD voltage during SITE was decreasing. By increasing the charge to the batteries prior to the fourth eclipse season, the EOD voltages for eclipse season 4 remained as high as those previously found for eclipse season 3. Discharge characteristics for eclipse seasons 5 and 6 show some additional degradation; however, battery performance continues to be excellent. The minimum battery voltage of 21.3 volts, after 3 years of daily discharges and eclipse cycling, still remains well above the 19-volt minimum required for power system operation.

The batteries are charged by the primary charge system which is a constant current ($C/10$) until the battery terminal voltage reaches a predetermined level as a function of temperature. At this point the battery current tapers, maintaining a fixed battery voltage. From the battery cell characterization test program, it was decided to set the battery voltage/temperature curve so that 95 percent ampere-hours of charge would be restored before the onset of taper. This minimized overcharge while allowing the batteries to become fully charged. Shown in figure 34 are actual flight data of the battery charge characteristics for eclipse season 1 and eclipse season 4. These data show that for eclipse season 4, the battery is starting taper after only 80 percent of the ampere-hours have been returned. From these data it is evident that the battery end-of-charge terminal voltage has increased causing premature taper. A contributing factor to this change in characteristic may be the large number of heavy noneclipse discharge cycles. Recognizing that premature taper was occurring, a method was required to fully charge the batteries. The recharge problem was solved with the standby (redundant) charger.

The standby battery charger provides a constant current charge of $C/20$ (0.75 ampere) to the battery and does not have voltage/temperature taper charge control. The power system has the flexibility to charge the battery from the primary charger, the standby charger, or by the parallel combination of both chargers. It was decided to charge the batteries initially from the main charger ($C/10$ rate) and allow the charge current to taper as normal; however, when the taper current reaches the $C/20$ rate, the charge control is switched to the standby charger to maintain the constant rate of $C/20$. The batteries complete charging on the standby charger. While use of the standby charger with its constant current rate resolved the charging problems, a multiple V/T level system would also do so. In addition, multiple V/T levels would provide added flexibility to accommodate further change in battery charge characteristics without sacrificing the charge taper characteristics.

After the battery charge problem was resolved, it was decided to evaluate battery capacity. This was accomplished by extending the SITE 2 experiment on February 22, 1976 (Day 53), which allowed the batteries to be discharged to 19.5 volts (1.02 V per cell) at an average discharge rate of approximately 2.5 amperes ($C/6$). The battery discharge characteristics for this test are shown in figure 35. A capacity of 13 ampere-hours was measured from this test. A similar test was performed on a group of five ATS-6 flight cells at NAD Crane. The results of this test are also shown in this figure.

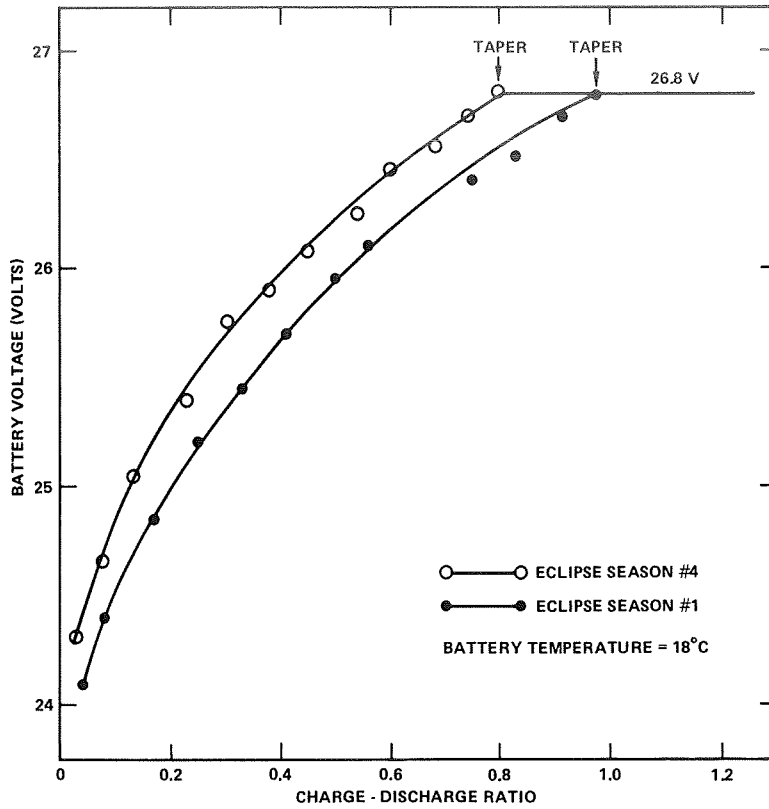


Figure 34. Battery charge characteristics.

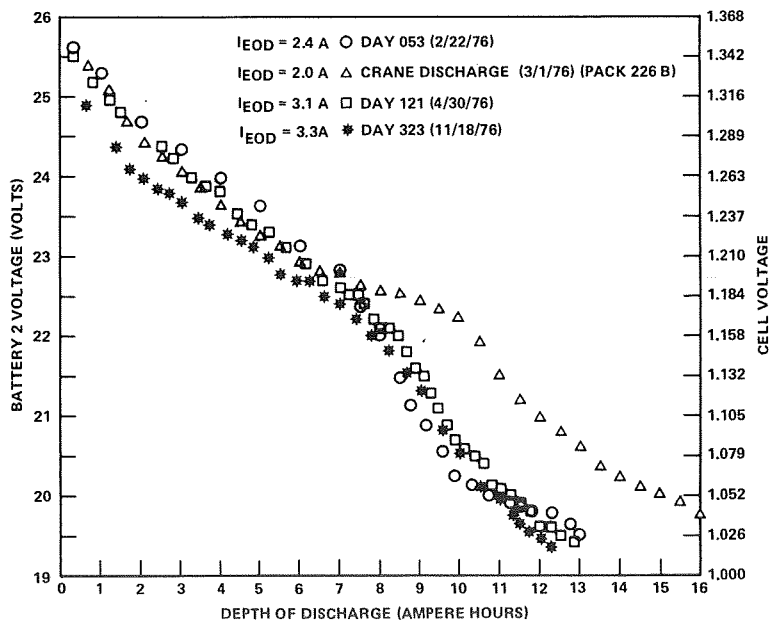


Figure 35. Discharge characteristics.

A comparison of the Crane flight cells to the spacecraft battery cells shows that additional degradation has occurred on the flight batteries. This is probably due to the additional non-eclipse cycles the spacecraft batteries have been subjected to that the Crane flight cells have not seen. A second deep discharge test was performed on April 30, 1976 (Day 121) following the fourth eclipse, about 70 days following the initial test. The results of that test are also shown in figure 35. While there were approximately 200 discharge cycles between the two tests, no appreciable degradation in capacity has occurred. This may be an indication that the rate of capacity loss has decreased significantly.

While the Crane cells have experienced some degradation, they have not experienced the equivalent degradation of the flight cells since they have been subjected to only 300 total discharge cycles. Of this total 170 cycles have been noneclipse discharges that simulated the actual profile experienced by the flight cells during SITE operations.

A third deep discharge test was performed on November 18, 1976 (Day 323), following the fifth eclipse season and the conclusion of the SITE experiment. Figure 36 shows this discharge characteristic. A capacity of 12 ampere-hours was measured. There was only a slight reduction of capacity in spite of the occurrence of an additional 275 discharge cycles.

The battery temperature varies daily between 10°C and 25°C with average temperatures of +18°C. Battery 1 and 2 temperatures have tracked within 1°C, and the battery voltages continue to share loads within 0.1 ampere.

Terminal voltages during discharge have tracked within 0.1 volt. Further, when the deep discharge tests were performed, battery 1 and 2 voltage continued to track within 0.1 volt until the tests were terminated at 19.5 volts. This indicates that the cells are still well matched with no apparent cell divergence.

CONCLUSIONS

The excellent performance and flexibility of the ATS-6 power system has contributed significantly to the successful operation of the spacecraft in carrying out its full complement of unique experiments. For almost three years, the power system has exceeded all operational requirements.

Of particular note are the following design and performance characteristics of the system:

- The power system shunt boost configuration was selected for efficient utilization of the array and battery power. It also provided a low impedance bus with excellent static and dynamic regulation. This characteristic was necessary to minimize load interactions and electromagnetic interference permitting the successful operation of multiple experiments.
- The array power degradation at the end of 2 years was 18.5 percent compared to 20 percent predicted. This performance has resulted in spite of the extreme eclipse cycling of -160°C to +60°C and the daily self-shadowing cycling of -100°C to 60°C. Therefore the adequacy of the array design and fabrication for a deployed array in synchronous orbit was verified.

- In the area of test, the large size of the solar array, consisting of 32 panels, posed a significant challenge for evaluating the array with accuracy and repeatability throughout the spacecraft test flow. A xenon flash illuminator coupled with a data evaluation system provided an improved method of solar array testing that allowed testing at the array, the panel, and the string level while the array was mounted on the spacecraft.
- The ATS-6 mission has required battery load sharing with the array on a daily basis. The batteries have been discharged to varying depths from 5 percent to 60 percent daily. Normally, for synchronous orbit, the batteries are required to support the spacecraft during the eclipse seasons only. The battery performance for this cycling regime has been good. There has been a small decrease in end-of-discharge voltage and a slight increase in end-of-charge voltage. Insufficient battery recharge resulted from this increase of end-of-charge voltage; however, with the flexibility designed into the charge system, reverting to the standby charger (C/20) resolved this problem. A multiple voltage-temperature level system would also solve the problem and accommodate further change in battery charge characteristics. Battery capacity has been evaluated through deep discharges to 1.02 V per cell at three different times during the second year of operation. The most recent test showed that after more than 1400 charge-discharge cycles, the batteries have 12.4 ampere hours of capacity versus a nominal capacity of 15 ampere hours. In spite of the severe battery usage, the batteries have still maintained a substantial amount of their initial capacity. This demonstrates that for synchronous orbits, batteries can be used for daily cycling in addition to normal use for eclipse cycling.

SOURCES

1. *ATS-F Data Book*, ATS Project, Goddard Space Flight Center, Greenbelt, Md., May 1974.
2. LaVigna, T., "The ATS-6 Power System—An Optimized Design for Maximum Power Source Utilization," presented at Tenth Intersociety Energy Conversion Engineering Conference Proceedings, 759157, August 18-22, 1975, Pg. 1048.
3. LaVigna, T., and K. Sizemore, "Design and Analysis of a Highly Efficient Power System for the Small Scientific Satellite (S³)," NASA GSFC Report X-716-69-540, November 1969.
4. Smith, A., T. LaVigna, and L. Pessin, "Design Impact of a Unique Solar Array Configuration for the ATS-F Electrical Power Subsystem," presented at Eighth IECEC, August 1973.
5. Smith, A., F. Hornbuckle, and F. Betz, "Evaluation of Flight Acceptance Thermal Testing for the ATS-6 Solar Array," presented at the 11th IEEE Photovoltaic Specialist Conference, 1975.

1. Report No. TP-1023	2. Government Accession No.	3. Recipient's Catalog No.	
4. Title and Subtitle The ATS-6 Power System: Hardware Implementation and Orbital Performance		5. Report Date September 1977	6. Performing Organization Code 733
		8. Performing Organization Report No. G-7703X10	
7. Author(s) Thomas A. LaVigna and Franklin L. Hornbuckle	9. Performing Organization Name and Address Goddard Space Flight Center Greenbelt, Maryland 20771		10. Work Unit No.
12. Sponsoring Agency Name and Address National Aeronautics and Space Administration Washington, D.C. 20546			11. Contract or Grant No.
			13. Type of Report and Period Covered Technical Note
		14. Sponsoring Agency Code	
15. Supplementary Notes			
16. Abstract The Applications Technology Satellite-6 has pushed the frontiers of health and education forward significantly by TV broadcast. It has performed more than 20 communications, technological and scientific experiments in almost 3 years of highly successful operation. Contributing substantially to this success has been the flexibility of the power system that allows multiple operation of experiments. The power system, a shunt-boost configuration, uses partial shunt regulation of the solar array and a boost regulator for control of battery power. Regulation is provided for three different operating modes: shunt, charge, and boost. This configuration achieves the highest efficiency of power transfer from the solar array to the loads. The excellent dynamic regulation and low output impedance of the power system virtually eliminated the problem of subsystem interactions on the power bus due to conducted interference from load current fluctuations. The performance of the power system continues to be excellent. The solar array degradation (18.5 percent) has been less than the specified 20 percent in two years in spite of extreme cycling from -160°C to 60°C. A unique battery cycling regime of discharges varying from 5 percent to 60 percent daily is being encountered. During the second year, noneclipse discharges have occurred twice a day to depths of 35 percent and 45 percent. Battery performance has been good with only a small decrease in end-of-discharge voltage. A recent test to evaluate capacity gave 12.4 Ah (83% of the nominal capacity of 15 Ah) after over 1400 battery discharge cycles. A small increase in the end-of-charge voltage has recently occurred necessitating a change in the charge regime to achieve full charge conditions.			
17. Key Words (Selected by Author(s)) Spacecraft power supplies, Satellite solar energy conversion, Electric batteries, Energy storage, Nickel-cadmium batteries		18. Distribution Statement Unclassified—Unlimited CAT. 20	
19. Security Classif. (of this report) Unclassified	20. Security Classif. (of this page) Unclassified	21. No. of Pages 39	22. Price* \$4.00

*For sale by the National Technical Information Service, Springfield, Virginia 22161.

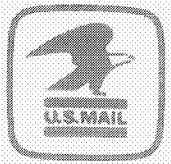
National Aeronautics and
Space Administration

Washington, D.C.
20546

Official Business
Penalty for Private Use, \$300

THIRD-CLASS BULK RATE

Postage and Fees Paid
National Aeronautics and
Space Administration
NASA-451



NASA

POSTMASTER: If Undeliverable (Section 158
Postal Manual) Do Not Return
